Glutamatergic Supramammillary Nucleus Neurons Respond to Threatening Stressors and Promote Active Coping

Abraham Escobedo[1], Salli-Ann Holloway[1], Megan Votoupal[2], Aaron L Cone[1], Hannah E Skelton[1], Alex A. Legaria[3,4], Imeh Ndiokho[5], Tasheia Floyd[6], Alexxai V. Kravitz[1,3,4], Michael R. Bruchas[7,8,9,10, *], Aaron J. Norris[1*]

Affiliations:

1 Department of Anesthesiology, Washington University in St. Louis, St. Louis, MO

2 Department of Medicine, Northwestern University Feinberg School of Medicine, Chicago IL

3 Department of Neuroscience, Washington University in St. Louis, St. Louis, MO

4 Department of Psychiatry, Washington University in St. Louis, St. Louis, MO

5 Medical College of Wisconsin, Milwaukee WI

6 Department of Obstetrics and Gynecology, Washington University in St. Louis, St. Louis, MO

7 Center for Neurobiology of Addiction, Pain, and Emotion University of Washington, Seattle, WA

8 Department of Anesthesiology and Pain Medicine University of Washington, Seattle, WA

9 Department of Pharmacology University of Washington, Seattle, WA

10 Department of Bioengineering University of Washington, Seattle, WA

* Corresponding authors

Lead Contact / Co-Corresponding:

Aaron Norris

660 S. Euclid Ave

Saint Louis, MO 63110

norris@wustl.edu

Co-Corresponding

Michael R. Bruchas

Seattle WA 98195

mbruchas@uw.edu

Abstract:

Threat-response neural circuits are conserved across species and play roles in normal behavior and psychiatric diseases. Maladaptive changes in these neural circuits contribute to stress, mood, and anxiety disorders. Active coping in response to stressors is a psychosocial factor associated with resilience against stress induced mood and anxiety disorders. The neural circuitry underlying active coping is poorly understood, but the functioning of these circuits could be key for overcoming anxiety and related disorders. The supramammillary nucleus (SuM) has been suggested to be engaged by threat. SuM has many projections and contains poorly understood diversity of populations. We identified a unique population of glutamatergic SuM neurons ($SuM^{VGLUT2+}$::POA) based on projection to the POA and found $SuM^{VGLUT2+}$::POA neurons have extensive arborizations. $SuM^{VGLUT2+}$::POA neurons project to brain areas that mediate various features of the stress and threat responses including the paraventricular nucleus thalamus (PVT), periaqueductal gray (PAG), and the habenula (Hb). Thus, $SuM^{VGLUT2+}$::POA neurons are positioned as hubs connecting to areas implicated regulating stress responses. Here we report $SuM^{VGLUT2+}$::POA neurons are recruited by diverse threatening stressors and recruitment of $SuM^{VGLUT2+}$::POA neurons correlated with active coping behaviors. We found that selective photoactivation of the $SuM^{VGLUT2+}$::POA population drove aversion but not anxiety like behaviors. Activation of $SuM^{VGLUT2+}$::POA neurons in the absence of acute stressors evoked active coping behaviors and drove goal directed behavior. Also, activation of $SuM^{VGLUT2+}$::POA neurons was sufficient to convert passive coping strategies to active behaviors during acute stress. These findings establish a new node in stress response circuitry that has projections to many brain areas and evokes flexible active coping behaviors and offers new opportunities for furthering our neurobiological understanding of stress.

Introduction

Threat-response neural circuits are conserved across species and have roles in normal behaviors and psychiatric diseases(*1-4*). Identifying and responding to threatening stressor is critical for survival but maladaptive changes in underlying neural circuits contribute to stress, mood, and anxiety disorders (*5, 6*). Active coping in response to stressors is psychosocial factor associated with resilience against stress induced mood and anxiety disorders(*7*). Available evidence indicates that active (e.g., escape, fighting) and passive (e.g., freezing, immobility) coping responses to stressors are governed by separable neural circuits (*1, 8, 9*). The functioning of circuits underling active coping could be key for overcoming anxiety and related disorders(*10, 11*).The neural circuits, cells, and mechanisms underlying active coping strategies remain unclear(*12, 13*).

The supramammillary nucleus (SuM) has been suggested to be engaged by threatening stressors and has efferent connections to stress-sensitive brain regions so may be an important regulator of responses to stressors (*14-16*). Research on SuM has focused on connections to the hippocampus and septum while SuM projections to other brain areas remain less understood(*15, 17, 18*). SuM contains distinct populations with functionally diverse roles including regulation of hippocampal activity during REM, spatial memory, arousal, and environmental interactions(*19-23*). In addition to functional diversity, anatomical and molecular-cellular diversity is present in SuM(*24-26*). Divergent populations in SuM have been defined by differential to the dentate gyrus and CA2 regions of the hippocampus, and neurochemically based on neurotransmitter expression (*27, 28*). Major projections from the SuM, which have yet to be examined, include the preoptic hypothalamus area (POA). We examined if SuM neurons projected to the POA and if this projection could be used to aid in separation of populations in SuM.

We used retrograde adeno associated viral (AAV) and combinatorial genetic tools to identify and characterize a population of glutamatergic SuM neurons with projections to the POA ($SuM^{VGLUT2+}$::POA). We found that $SuM^{VGLUT2+}$::POA neurons represented an anatomical subset of SuM neurons with extensive arborizations to brain regions including that mediate stress and threat responses including the paraventricular nucleus (PVT), periaqueductal gray (PAG), and the habenula (Hb). Thus, $SuM^{VGLUT2+}$::POA neurons are positioned as hubs with spokes to many areas regulating responses to threatening stressors. We hypothesized this population could respond to and regulate responses to stressors. We found $SuM^{VGLUT2+}$::POA neurons are recruited by multiple types of acute threatening stressors, encode a negative valance, do not promote anxiety-like behaviors, and evoke active coping behaviors. Further, activation of these $SuM^{VGLUT2+}$::POA neurons was sufficient to convert passive coping strategies to active behaviors.

These findings indicate SuM$^{VGLUT2+}$::POA neurons are a central hub linked to multiple stress and threat responsive areas and can drive state transitions between passive and active responses to stress.

Results

VGLUT2+ SuM neurons projecting to the POA (SuM$^{VGLUT2+}$::POA) arborize to multiple stress-engaged brain regions

The SuM contains functionally diverse and anatomically distinct populations with efferent projections to many brain regions(*16, 24, 38, 39*). The diversity includes glutamatergic, GABAergic, and co-expressing GABAergic/Glutamatergic populations(*21, 40*). Using retrograde adeno associated virus (Retro-AAV) (Retro-AAV2-DIO-tdTomato) and anterograde (AAV5-DIO-ChR2eYFP) tracing we identified a population of VGLUT2+ expressing neurons in SuM that project to the POA (SuM$^{VGLUT2+}$::POA) with dense projections in the lateral preoptic area (LPO) within the POA (**Supplemental Figure 1A-F**) in VGLUT2-Cre mice (n=4). Using a viral construct encoding for a nuclear restricted fluorophore that switches from mCherry (red) to eGFP (green) in a Cre-dependent manner (Retro-AAV2-Nuc-flox(mCherry)-eGFP) we found SuM$^{VGLUT2+}$::POA neurons were positive for VGLUT2+ in VGLUT2-Cre mice (n=4) and negative for VGAT expression in VGAT-Cre mice (n=3) (**Supplemental Figure 1G-L**) indicating that SuM$^{\mathbf{VGLUT2}}$::POA neurons do not belong to a GABAergic/Glutamatergic populations.

To examine arborization of SuM$^{VGLUT2+}$::POA neurons we utilized a combinatorial genetic approach. Specifically, we used mice (VGLUT2-Flp) that express Flp recombinase in VGLUT2 expressing cells in a combination with Flp dependent expression (fDIO) of Cre and Cre (DIO) dependent fluorophore expression. We injected Retro-AAV2-DIO-eYFP into POA and AAV-fDIO-Cre in to SuM (**Figure 1A**). We thus expressed Cre in SuM$^{VGLUT2+}$ neurons and, of those, only neurons projecting to the POA (SuM^{VGLUT2}::POA neurons) were labeled with eYFP. We found SuM^{VGLUT2}::POA neurons arborize widely projection to multiple brain regions including: the nucleus accumbens (Acb), Septum, lateral hypothalamus (LH), ventral medial hypothalamus (VMH), paraventricular nucleus (PVT), lateral habenula (lHb), the ventral lateral periaqueductal gray (VLPAG), dorsal raphe (DRD), lateral parabrachial nucleus (LPBN), laterodorsal tegmental nucleus (LDTg), and medial vestibular nucleus (MVe) (**Figure 1 D-M**). We visualized arborization of SuM^{VGLUT2}::POA neurons in cleared tissue by using optical light sheet imaging. For these experiments we injected VGLUT2-Flp mice (n=3) we injected as in Figure 1A and brains were actively cleared using SHIELD for optical light sheet imaging(*42*). Compiled three-dimensional images of a brain hemisphere, viewed from the medial to lateral perspective (**Figure 1M**) or

viewed from the ventral to dorsal perspective (**Supplemental Figure 2M**), showed projections labeled by eYFP from SuM$^{VGLUT2+}$::POA to POA, areas of hippocampus, septum, Acb, and regions in the pons and midbrain. The results further established projections from SuM$^{VGLUT2+}$::POA neurons to multiple brains areas and illustrate the broad arborization.

We used tracing with Retro-AAV's to confirm our findings from anterograde tracing by injecting unilaterally into the Acb, septum, PVT, or PAG in VGLUT2-Cre mice. Cell bodies in SuM were labeled eYFP or tdTomato (**Supplemental Figure 2A-L**). Each area was injected in three or more mice yielding similar results. We examine anatomic distribution of SuM::POA neuron in SuM by injected Retro-AAV2-Cre into the POA and Retro-AAV2-Nuc-flox(mCherry)-eGFP into the SuM (**Supplemental Figure 3 A-B**) of wildtype (WT) Cre- mice (n=3) injected with this combination of viruses we observed both neurons labeled by mCherry (Cre negative) or eGFP (Cre expressing) interspersed in the SuM. We verified the combinatorial viral selectively labeled SuM$^{VGLUT2+}$::POA neurons with minimal background(*43*). Positive controls we injected Retro-AVV-Flpo into the POA and AAV-fDIO-Cre into the SuM labeling of cells in SuM (**Supplement Figure 3 G and H**). As negative controls, we injected only AVV-fDIO-Cre into the SuM in Ai14 mice, which did not yield tdTomato expression (**Supplemental Figure 3C-D).** To confirm that the combination of Retro-AAV2-fDIO-Cres and AAV5-DIO-ChR2eYFP did not lead to labeling of cells with eYFP in the absence of Flp we injected Retro-AAV2-fDIO-Cre into the POA and AAV-DIOChR2eYFP into SuM of WT mice. In these mice we did not observe any expression of eYFP (**Supplemental Figure 3E-F**). The results demonstrate the specificity of our combinatorial viral strategy. All studies replicated in a minimum of three mice.

SuM$^{VGLUT2+}$::POA neurons are an anatomical distinct subset of all SuM$^{VGLUT2+}$ neurons.

Recent studies have highlighted functionally divergent roles of SuM neurons and suggested differential projections, particularly to regions of hippocampus and PVT, may identify functionally distinct populations (*19, 20*). To examine if SuM$^{VGLUT2+}$::POA neurons are a subset of SuM$^{VGLUT2+}$ neurons we qualitatively compared the projections of total SuM$^{VGLUT2+}$ neurons to SuM$^{VGLUT2+}$::POA neurons. Similar to projections for SuM$^{VGLUT2+}$::POA neurons (**Figure 1**) we observed labeled projections from the total SuM$^{VGLUT2+}$ neurons in the POA, PVT, LHB, and the CA2 field of the hippocampus (**Figure 2 A-E**). Importantly, we found areas that received projections from the total SuM$^{VGLUT2+}$ and not from SuM$^{VGLUT2+}$::POA neurons. As schematized (**Figure 2K**), projections from the total SuM$^{VGLUT2+}$ but not SuM$^{VGLUT2+}$::POA populations were present in dentate gyrus (DG) and medial habenula (mHb) (**Figure 1G and Figure 2 F-J**). Thus, SuM$^{VGLUT2+}$::POA population can be further defined as a subset of the total SuM$^{VGLUT2+}$ neuronal

101 population with distinct projection targets. Some areas, such as septum, may receive projections
102 from multiple populations.

103 **Threatening stressors not spontaneous higher velocity movement recruit SuM$^{VGLUT2+}$::POA**
104 **neurons**

105 Neurons in SuM can be activated by acute stressors, and we sought examine the
106 recruitment of SuM$^{VGLUT2+}$::POA neurons by threatening stressors (*14, 44, 45*). We found that
107 forced swimming induced cFos expression in SuM. Labeling SuM$^{VGLUT2+}$::POA neurons using
108 Retro-AAV-DIO-mCherry revealed an increase in the number of mCherry and cFos labeled cells
109 following forced swim (**Supplemental Figure 4A-G**). To further examine recruitment of
110 SuM$^{VGLUT2+}$::POA neurons by acute stressors we tested a diverse set of acute threatening
111 stressors using *in vivo* Ca^{2+} detection via fiber photometry. We expressed GCaMP7s in
112 SuM$^{VGLUT2+}$::POA neurons (**Figure 3A-B**) using the combinatorial viral genetic approach detailed
113 for anatomic studies. We developed a forced swim assay that utilized a moveable platform
114 allowing mice to be placed into and removed from water while obtaining fiber photometry
115 recordings. Mice were dunked for a 30-second swim trial every 2 minutes for a total of 10 trials
116 (n=8 mice). During the assay mice exhibited almost exclusively active swimming and climbing
117 behaviors reflected in the quantification of mean time mobile (**Supplemental Figure 4I**). Analysis
118 of Ca^{2+}dependent (470 nm excitation) and isosbestic control (415 nm excitation) signals from fiber
119 photometry recordings reveal rapid rise of approximately 5 standard deviations in GCaMP Ca^{2+}
120 dependent signal with start of the swim trial that was sustained through the 30-sec swim period.
121 The Ca^{2+}dependent signal returned to baseline following the platform raising removing the animal
122 from the water (**Figure 3F and G**). These data show the dunk assay evoked active coping
123 behavior and recruited SuM$^{VGLUT2+}$::POA neurons.

124 We also tested a foot shock paradigm (**Figure 3D**) and a predator ambush assay (**Figure**
125 **3E**). In foot shock assays VGLUT2-Flp mice (n=6), prepared as above (**Figure 3A and B**), were
126 subjected to five pseudo randomly spaced trials with 30 sec of tone proceeding a two-second
127 shock. We observed a rapid increase in the Ca^{2+} dependent GCaMP7s signal following the foot
128 shock (**Figure 3H and I**). For the predator ambush we adapted a previously demonstrated
129 paradigm using a mock mechanical spider attack (*46*). In this assay a remote-controlled
130 mechanical spider was hidden in a box with swing door. The box was inside a larger walled arena.
131 Mice were able to freely explore the arena and at a moment when the mouse was in proximity to
132 the box opening the spider was moved out towards the mouse. The mice fled, often to a corner,
133 stopped, turned to face the spider (**Supplemental video 1**). In mice (n=9) subjected to the

134 ambush paradigm we observed an increase in Ca^{2+} dependent GCaMP signal at the time of the
135 ambush followed by suppression below the initial baseline (**Figure 3J**). Populations of neurons in
136 SuM have previously been found to correlate with future movement velocity (*41*), so we examined
137 if recruitment of $SuM^{VGLUT2+}$::POA neurons was correlated to periods of spontaneous higher
138 velocity movement. Analyzing data collected prior to the ambush event we examined if increased
139 velocity, at speeds similar to the fleeing induced by the ambush, was correlated with increased
140 Ca^{2+} dependent GCaMP signal in $SuM^{VGLUT2+}$::POA neurons (**Figure 3L**). We found no correlation
141 (**Figure 3K**). We further examined the data for a correlation of increased Ca^{2+} dependent signal
142 in $SuM^{VGLUT2+}$::POA neurons to movement velocity during open field exploration in a sperate
143 cohort of mice (n=13). Here we found no evidence for correlation of velocity with Z-score of Ca^{2+}
144 dependent signal including a cross correlation analysis to account for a potential temporal offset
145 (**Supplemental Figure 5**). In aggregate, the data support recruitment of $SuM^{VGLUT2+}$::POA
146 neurons by diverse threatening stressors but not during times of higher velocity spontaneous
147 movement.

148 **$SuM^{VGLUT2+}$::POA neurons evoke active coping behaviors**

149 To examine how activation of $SuM^{VGLUT2+}$::POA neurons contributes to responding to
150 threatening stressors we assessed behavioral changes evoked by photostimulation of
151 $SuM^{VGLUT2+}$::POA neurons. We injected VGLUT2-Cre or WT (Cre-) mice with Retro-AAV5-DIO-
152 ChR2eYFP in the POA, and an optic fiber placed over SuM (**Figure 4A**). We employed a
153 paradigm with a 15-minute trial divided into three 5-minute periods, pre-stimulation, stimulation at
154 10 Hz, and post-stimulation. Based on review of videos obtained during the 15-min trials, we
155 observed behaviors that could be classified into nine distinct categories: grooming, immobile,
156 walking, chewing of bedding, rearing, rapid locomotion (movement was limited by the size of the
157 arena), digging (moving bedding towards the tail), treading (moving bedding forward with front
158 paws), and jumping (**Figure 4B**). A blinded observer scored the behaviors in 10-second intervals
159 for the predominant behavior observed during each interval and each behavior was assigned a
160 color for visualization. Color coded representation of trials from 16 Cre+ (n=16) and WT (n=16)
161 mice is illustrated (**Figure 4B**). The behavioral pattern in the pre-stimulation period is similar
162 between the Cre+ and WT mice. During the stimulation period, a clear shift in behavior was
163 evident in Cre+ mice. Photostimulation induced rearing, treading, digging, rapid locomotion, and
164 jumping. During the post-stimulation period we observed a new pattern with Cre+ mice spending
165 time immobile and grooming. An example of a Cre+ animal is shown in **Supplemental video 2**.

166 We analyzed behavior quantifying specific behaviors during each period. Quantification of
167 jumping revealed that Cre+ mice (n=16) engaged in significantly (p=0.0012) more jumps during
168 the stimulation period compared to WT (n=16) mice (**Figure 5C**). During the pre- and post-
169 stimulation periods there was not a significant difference in the number of jumps. We also
170 observed that during the stimulation period the Cre+ mice engaged in bouts treading/digging,
171 vigorously moving bedding forwards and backwards, as previously described for defensive
172 burying (*47*). Defensive burying, characterized by moving bedding forward or backwards often in
173 alternating pattern, is evoked by threatening and noxious stimuli, and is a described active stress
174 coping strategy in rodents(*47-50*). We conservatively quantified together the movement of
175 bedding as treading/digging that may include spontaneous digging (**Figure 4D**) and found no
176 significant (p=0.7) difference during the pre-stimulation period. In the stimulation period there was
177 a significant (p=0.004) increase in the time spent treading/digging, and surprisingly, during the
178 post-stimulation period time treading/digging was significantly (p=0.0028) decreased in Cre+
179 mice. The variability in behaviors can be attributed to exclusion of one behavior by the other, with
180 individual mice having variability in the predominant behavior displayed during the
181 photostimulation period but all mice shifted to increased activity coping behaviors. The behaviors
182 evoked by photostimulation fit with active coping behaviors. Specifically, escape (jumping, rapid
183 locomotion), defensive burying/treading (digging, pushing beading forward).
184 We also quantified grooming behaviors in each of the three periods (**Figure 4E**). During
185 the pre-stimulation period there was not a significant difference. During the stimulation period the
186 Cre+ mice did not engage in grooming leading to a significant (p<0.0001) decrease in time spent
187 grooming compared to Cre- mice. In the post-stimulation-period Cre+ mice showed a significant
188 (p<0.0001) increase in time spent grooming compared to Cre- mice. A reasonable interpretation
189 of rise in grooming post stimulation is that photostimulation evoked a stressed like state and
190 cessation of photostimulation led to selfcare grooming as seen following acute stressors (*51, 52*).
191 In summary, the analysis of behaviors elicited by photostimulation of $SuM^{VGLUT2+}$::POA neurons
192 without conditioned cues or concomitant stressors demonstrates a dramatic shift in behavior to
193 escape oriented (jumping, rapid locomotion) and threat response behavior, including rearing and
194 defensive burying, during the photostimulation period. In contrast to freezing, the behaviors
195 elicited by activation of $SuM^{VGLUT2+}$::POA neurons indicate that they alter active coping strategies.

196 **Photostimulation of $SuM^{VGLUT2+}$::POA neurons drives real-time avoidance**

197 To examine whether activation of $SuM^{VGLUT2+}$::POA neurons may contribute to the aversive
198 aspects of threatening stress we carried out real-time place aversion testing (RTPA) by pairing

199 one side of the chamber with photostimulation of SuM$^{VGLUT2+}$::POA (**Figure 5A**) neurons at
200 multiple frequencies (1,5,10, and 20 Hz). Photostimulation of SuM$^{VGLUT2+}$::POA neurons produced
201 significant ($p<0.0001$) aversion at all frequencies in Cre+ (n=19) mice compared to Cre- (n=21)
202 control and higher stimulation frequencies evoked greater aversion (**Figure 5B and C**). Example
203 of Cre+ mice with stimulation at 1, 5, and 10Hz as well as Cre- mice is in **Supplemental Video**
204 **3**. WT and Cre+ mice explored equivalently, with similar ($p=0.87$ mixed-effects model) number of
205 entries to the stim side (**Figure 5D**). Cre+ mice quickly left the simulation side and the mean time
206 spent on the stimulation side of the area was significantly ($p<0.0001$) lower (**Figure 5E**). These
207 data indicate surprisingly that photostimulation, although aversive, did not generate aversive
208 pairing, as found for other brain areas (*53*). To examine the relative aversiveness of
209 SuM$^{VGLUT2+}$::POA photostimulation we carried out RTPA experiments using an arena with a dark
210 side and a bright side (**Figure 5F inset**). We paired photostimulation with the dark side. As
211 expected, Cre- mice show a preference for the dark side of the arena (**Figure 5F**), however
212 photostimulation of the SuM$^{VGLUT2+}$::POA neurons yielded significant (1 Hz $p=0.002$, 5 Hz
213 $p=0.0004$, and 10 ,20 Hz $p<0.0001$) aversion of Cre+ (n=13) compared to Cre- (n=12). Cre+ mice
214 spent nearly the entire trial in the brightly light side demonstrating photostimulation of
215 SuM$^{VGLUT2+}$::POA neurons drove avoidance sufficient overcome a mildly aversive stimulus (bright
216 light).

217 Reports have described multiple populations of neurons in supramammillary including
218 neuronal populations that project to the dentate gyrus of the hippocampus that release both GABA
219 and glutamate. Our anatomic studies indicated that SuM$^{VGLUT2+}$::POA neurons do not project to
220 the dentate gyrus (**Figure 2**) and are not GABAergic (**Supplemental Figure 1G-L**). Thus,
221 SuM$^{VGLUT2+}$::POA neurons are not part of either a GABAergic or dual transmitter population. To
222 examine if GABAergic neurons in SuM (SuM^{VGAT+}) can mediate real-time place aversion or
223 preference, we injected VGAT-Cre mice with AAV to express ChR2 (n=26) or control (n=26) in
224 SuM and carried out real-time place aversion testing. Photostimulation at 10 Hz yielded no
225 significant aversion or preference compared to baseline (**Supplemental Figure 6A-D**). This is in
226 contrast to the robust aversion caused by photostimulation of SuM$^{VGLUT2+}$::POA neurons.

227 **Photoactivation of SuM$^{VGLUT2+}$::POA neurons does not cause anxiogenic-like behavior**

228 Threat can induce anxiety-like, risk aversion behavioral states (*54-56*). To test whether
229 activity of SuM$^{VGLUT2+}$::POA neurons contributes to anxiety-like behaviors we used two established
230 assays for anxiety-like behavior, open field, and light-dark exploration (*57-60*). During open field
231 testing 10 Hz photostimulation was applied to SuM$^{VGLUT2+}$::POA neurons. We quantified the time

232 spent in the perimeter (outer 50%) vs. the center (inner 50%) of the arena and found VGLUT2-
233 Cre+ (n=18) and WT (n=17) mice did not significantly (p=0.17, and 0.19) differ (**Figure 5G and**
234 **H**). The total distance traveled was significantly (p<0.001) increased in in Cre+ mice compared to
235 WT mice (**Figure 5I**). Increased distance traveled in some mice was not surprising, because prior
236 testing (**Figure 4**) revealed the mice engaged in escape behaviors during photostimulation. We
237 observe behaviors including jumping during open field testing as well. We also carried out open
238 field testing using VGAT-Cre mice to selectively activate SuM^{VGAT+} neurons and observed no
239 significant (p=.99) effect on time in center or perimeter (**Supplemental Figure 6F**), but mice
240 expressing ChR2eYFP displayed a small but significant (p=0.035) decrease in distance traveled
241 **(Supplemental Figure 6G)**. We tested if photostimulation of $SuM^{VGLUT2+}$::POA neurons would
242 increase preference for the dark area, a potential sign of elevated anxiety (**Figures 5J**). We found
243 photostimulation of $SuM^{VGLUT2+}$::POA neurons did not significantly(p=0.9) alter preference (**Figure**
244 **5K**) in VGLUT2-Cre+ mice (n=8) compared to WT (n=9). The activation of $SuM^{VGLUT2+}$::POA
245 neurons evoked escape behaviors in open field testing, as seen in Figure 4, leading to a significant
246 (p=0.003) increase in total distance moved (**Figure 6L**). The findings we obtained in open field
247 and light-dark exploration testing do not support a role for $SuM^{VGLUT2+}$::POA neurons in driving
248 anxiety-like behaviors.

249 **$SuM^{VGLUT2+}$::POA neurons can drive instrumental action-outcome behavior**

250 Current theoretical frameworks for examining threat responses divide behaviors into two
251 broad categories, innate (fixed) and instrumental (action-outcome)(*1, 61*). Additionally, stress
252 responses can be divided into active vs passive actions. Behaviors in these separable categories
253 are mediated by distinct neural circuits(*1, 62*). For example, areas involved in responding to
254 specific threatening stimuli (looming threat) drive an innate fixed behavior repertoire(*10*).
255 Photostimulation of $SuM^{VGLUT2+}$::POA neurons evoked multiple active behaviors displayed when
256 responded to threatening or noxious stimuli (**Figure 4**). To test if $SuM^{VGLUT2+}$::POA neurons can
257 promote flexible repertoires of behavior including goal-directed, as opposed to only innate
258 behaviors (ex. fleeing), we used an operant negative reinforcement paradigm (**Figure 6A-B**).
259 Because our results show photostimulation of $SuM^{VGLUT2+}$::POA neurons is aversive
260 photostimulation of $SuM^{VGLUT2+}$::POA neurons could be used as a negative reinforcer. We
261 hypothesized if stimulation of $SuM^{VGLUT2+}$::POA evokes fixed innate defensive behaviors, or simply
262 promotes high amounts of locomotion, then performance of an operant task (an action-outcome
263 behavior) would be impaired because these behaviors would conflict with performance of the
264 operant task. Importantly, results obtained can help differentiate general elevation in locomotor

activity from directed coping behavior. We employed a paradigm using two nose poke ports, one active and one inactive. SuM$^{VGLUT2+}$::POA neurons were photostimulated at 10 Hz during a 10-minute trial. Activation of the active port by a nose poke triggered a 10-second pause in photostimulation and turned on a house light for 10 sec (**Figure 6A and B**). Following this 10-sec pause the house light switched off and photostimulation resumed until the subsequent activation of the active port. We tested animals for 4 consecutive days with the 10-min trials without prior training. Importantly, performance of the task had to be completed during photostimulation.

Analyses of port activations during the 10-min trials revealed that Cre+ mice (n =11) paused the photostimulation (reward) significantly ($p<0.0001$) more on all four days of testing compared to Cre- (n=11) mice (**Figure 6C**). The number of 10-second pauses approached the maximum, 60 possible in a 10-min period. Cre+ mice engaged the active port significantly ($p<0.001$) more than Cre- mice (**Figure 6D**). Indicating no difference in baseline performance of the task, the time to the first engagement of the active port was not significantly ($p=0.32$) different for Cre+ compared to Cre- mice during the first test trial. During the three subsequent tests Cre+ mice were significantly ($p<0.01$) faster to engage the active port after the start of the trial compared to Cre- mice. Cre+ mice also were significantly ($p<0.01$ paired t-test) faster in trials two through four at engaging the active port compared the first trial. Interestingly, Cre+ mice engaged the active port significantly ($p=0.009$ paired t-test) fewer times on the fourth day than the first day but achieved more pauses (**Figure 6E**).

To examine effort-related motivation we employed a 30-min test using a progressive ratio requiring exponentially increasing number of active port activations to trigger a pause in the photostimulation on the fifth day of operant behavior testing **(Figure 6B**) (*63*). During trials using a progressive ratio, Cre+ mice activated the active port and paused stimulation significantly ($p<0.001$) more times than Cre- mice (**Figure 6F**). Examination of individual cumulative active port activation data showed Cre+ mice continue to engage the active port throughout progressive ratio trials despite the increasing work required to generate each pause in photostimulation. No breakpoint was observed during the trial (**Figure 6G and H**). This finding indicates that activation of SuM$^{VGLUT2+}$::POA neurons remains salient and motivating through the tested period and that photostimulation of does not evoke behaviors precluding completion of the task. Examination of reward behavioral epochs for representative animals shows that for lowest total number of rewards earned (green dots) the next pause required 20 activations of the active port and for the highest (red dots) the next pause required 50 activations of the active port. Taken together, results from instrumental reinforcement tasks demonstrate that activation of SuM$^{VGLUT2+}$::POA neurons

298 does not solely evoke innate stereotyped behaviors and can drive active coping in the form of
299 instrumental behaviors.

300 **SuM$^{VGLUT2+}$::POA neurons are recruited during active coping behaviors in forced swim**
301 **testing**

302 The forced swim test is increasingly understood as an assay of coping strategy with
303 passive and active components (*64, 65*). During a first trial of forced swimming mice shifted from
304 active escape behaviors (wall climbing, robust swimming) to in passive (immobile floating)
305 behaviors. We found that SuM$^{VGLUT2+}$::POA neurons were recruited in a short dunk assay (**Figure**
306 **3F and G**), which elicited active escape behaviors (**Supplemental Figure 4A**). To test if
307 recruitment of SuM$^{VGLUT2+}$::POA neurons changes with the shift from active to passive behaviors
308 during a longer swim assay we carried out experiments using fiber photometry paired with
309 automated computer-based behavior analysis(*66*). The automated behavior scoring enabled high
310 temporal resolution analysis of behaviors (**Supplemental Video 4**) and each frame of the video
311 was coded for the classified behavior and plotted as color coded point. We observed 4 types of
312 behavior during forced swimming: climbing, swimming, hindpaw swimming, and immobile floating
313 and trained a model to identify each. Analysis of behavior showed that after the first minutes of
314 the trial mice shifted from swimming and climbing to immobile floating with intermittent swinging
315 or hindpaw swimming. We examined if recruitment of SuM$^{VGLUT2+}$::POA neurons changed in
316 correlation with this shift to more passive behavior. As shown in representative trace (**Figure 7A**)
317 the Ca^{2+}-dependent signal decreased the shift in behavior was occurring. To combine behavioral
318 data we assigned numerical values, one through four, to each behavior: climbing (4), swimming
319 (3), hindpaw swimming (2), and immobile floating (1). The mean was plotted as a heat map (red
320 higher values to blue lower values) to be compared to time locked fiber photometry data (**Figure**
321 **7B**). Examining the timeframe around the behavioral shift in each animal we found that as
322 behavior shifted from active coping (climbing, swimming) to more passive strategies and greater
323 immobility the Ca^{2+} signal substantially declined (**Figure 7B**). Examining data after this initial
324 transition we observed that many elevations in the Z-score were accompanied by changes in
325 behavior to swimming or hindpaw swimming (**Figure 7A**). To further examine this possible
326 correlation, we examined the time frame around transition to hindpaw swimming for changes in
327 Ca^{2+} signal. In a 20-sec window centered on the onset of hindpaw swimming we hind swimming
328 was accompanied by a rise in the Ca^{2+} dependent signal across multiple events within a trial
329 (**Figure 7C**). A similar analysis across events in multiple animals demonstrated a similar rise in
330 the Ca^{2+} dependent signal from SuM$^{VGLUT2+}$::POA neurons during the shift from immobility to

331 hindpaw swimming or swimming behaviors (**Figure 7D**). Time series analysis of 20-sec epochs
332 centered on random time intervals did not reveal any rise in the Ca^{2+} dependent signal (**Figure**
333 **7E**). These data indicate that recruitment of $SuM^{VGLUT2+}$::POA neurons fluctuates with changes in
334 coping strategy during a forced swim assay with decreased engagement of this circuit during
335 times of immobility.

336 **$SuM^{VGLUT2+}$::POA neurons promote active coping during forced swim test**

337 We found that $SuM^{VGLUT2+}$::POA neurons are activated by acute stressors (**Figure 3**), are
338 recruited during times of greater active coping behaviors (**Figure 7**). To test if $SuM^{VGLUT2+}$::POA
339 neurons can drive a switch in coping strategy in the context of ongoing stressor we used a two-
340 day forced swim stress test (*65, 67*). We tested animals during the second day, when immobile
341 floating is the predominant behavior. As in previous experiments, we used VGLUT2-Cre (Cre+)
342 or WT (Cre-) mice injected in the POA bilaterally with Retro-AVV-DIO-ChR2eYFP. On day one
343 we subjected mice to 15 mins of forced swim. On the subsequent day we repeated the forced
344 swim for six mins divided into three periods, pre-stimulation, stimulation at 10Hz, and post-
345 stimulation (**Figure 7F**). Trials on the second day were recorded and scored by a blinded observer
346 for time spent immobile in each 2-min period. Example of Cre+ mouse with stimulation 10Hz is
347 shown in **Supplemental Video 3**. During the pre-stimulation period Cre+ (n=9) and Cre- (n=11)
348 mice there was not a significantly (p=0.45) different amount of time immobile. During the
349 stimulation period Cre+ mice began swimming and attempting to climb the wall of the circular
350 swim arena, reflected by significantly (p<0.0001) less time immobile (**Figure 7H**). Interestingly, in
351 the post stimulation phase the difference in time spent immobile between Cre+ can WT mice
352 decreased but remained significantly (p=0.016) different. These results indicate that in the context
353 of an ongoing stressor activation of $SuM^{VGLUT2+}$::POA neurons is sufficient to trigger a change in
354 coping strategy from a largely passive (floating) to and active (swimming, climbing). The persistent
355 effect of the acute activation into the poststimulation phase suggests that activation of
356 $SuM^{VGLUT2+}$::POA neurons may shift how the stressor is processed or approached.

357 We next examined the effect of 10 Hz photostimulation of SuM^{VGAT} neurons on coping
358 strategy using the same two-day swim paradigm. VGAT-Cre mice were injected in the SuM to
359 express ChR2eYFP (n=10), or control (eYFP) (n=11) and a fiber optic was placed over SuM
360 (**Figure 7F**). Quantification of behavior revealed no significant difference in time spent immobile
361 during the pre-stimulation or the stimulation periods. Surprisingly, in the post-stimulation period
362 we observed a dramatic shift in behavior marked by significant (p=0.0004) decrease in time spent
363 immobile (**Figure 7I**). The amplitude of change in behavior was similar as we observed during the

364 stimulation phase of the experiments on SuM$^{VGLUT2+}$::POA neurons (**Figure 7H**). One
365 interpretation of these data is that release of sustained local inhibition leads to rebound activity of
366 output SuM$^{VGLUT2+}$::POA neurons.

367 **Suppression of SuM$^{VGLUT2+}$::POA neurons is required for feeding**

368 Feeding and responding to threats are conflicting actions and SuM$^{VGLUT2+}$::POA neurons
369 may play a role in switching between behavioral paradigms (e.g., feeding vs escape). We have
370 found threatening stressors recruit SuM$^{VGLUT2+}$::POA neurons. Responding to an acute
371 threatening stressor would prevent feeding. We sought to examine SuM$^{VGLUT2+}$::POA neuron
372 activity in relation to feeding using fiber photometry. To promote varying drive for food mice were
373 given *ad lib* access to food (fed condition) or food deprivation for 24 hours and on testing day
374 presented with a chow pellet while Ca^{2+} dependent and isosbestic signals were recorded. In the
375 fed state mice spent significantly ($p<0.001$) less time interacting with the food (**Figure 8C**) and
376 ate significantly ($p<0.001$) less (**Figure 8D**) compared to food deprived state. We analyzed the
377 Ca^{2+} dependent and isosbestic signals around presentation of food to fed and food deprived mice.
378 In the food deprived state mice spent more time with the food and ate more food (**Figure 8E and**
379 **F**). At the time of food presentation, the Ca^{2+} dependent signal decreased but not the isosbestic
380 signal. The change in the Ca^{2+} dependent was larger in the food deprived state (**Figure 8E and**
381 **F**). Together this data supports suppression of SuM$^{VGLUT2+}$::POA neural activity during
382 consummatory behavior with greater consumption associated with greater suppression.

383 To examine whether activation of SuM$^{VGLUT2+}$::POA neurons disrupted consummatory
384 behavior we tested the impact of photostimulation on feeding behavior in food deprived mice.
385 Using VGLUT2-Cre (Cre+) or WT (Cre-) mice injected with Retro-AAV5-DIO-ChR2eYFP into the
386 POA and implanted with a fiber optic midline over SuM we examined how feeding behaviors in
387 food deprived mice were altered by 10 Hz photostimulation of SuM$^{VGLUT2+}$::POA neurons (**Figure**
388 **8G- and D**). We used trials lasting 20 mins with unrestricted access to food added at the start of
389 the trial. Each trial was divided into three periods, a 5-min pre-simulation period, 10-min
390 stimulation period, and a 5-min post-stimulation period. Trials were recorded and scored for time
391 spent interacting with the food pellet. During the pre-stimulation period Cre+ ($n=17$) and Cre-
392 ($n=16$) mice spent interacting with the food was not significantly ($p=0.37$) different. With the start
393 of photostimulation the Cre+ mice stopped eating and interacting with the food. During the
394 stimulation period Cre+ mice spent significantly ($p=0.0002$) less time interacting with the food
395 compared to Cre- mice. Surprisingly, the decrease in time spent interacting with food continued
396 into the post-stimulation phase when Cre+ mice interacted with the food significantly ($p<0.0001$)

397 less (**Figure 8E**). Reflecting the decrease in time spent with the food, Cre+ mice consumed
398 significantly (p=0.001) less food during the 20-min trial than Cre-mice. These results indicate that
399 SuM$^{VGLUT2+}$::POA neurons can redirect behavior away from consumption and suppression of
400 SuM$^{VGLUT2+}$::POA neurons is required for feeding even in a food deprived state. Ethologically,
401 animals must choose rapidly between responding to threats and feeding when foraging. The
402 findings here implicate this pathway in control of switching between these behaviors.

403 **Discussion**

404 The presented data show SuM$^{VGLUT2+}$::POA population of neurons have broad
405 arborizations to brain regions involved in responding to threat and stress (**Figures 1, 2, and**
406 **Supplemental Figure 2**), are recruited by threatening stressors (**Figures 3 and 7**), can contribute
407 to multiple aspects of behavioral responses to threatening stressors, and promote active coping
408 behaviors (**Figures 6 and 7**). We also found that SuM$^{VGLUT2+}$::POA can drive aversion and
409 although aversive stimuli can promote anxiety-like behaviors, photostimulation of
410 SuM$^{VGLUT2+}$::POA stimulation did not (**Figure 5**). This finding suggests SuM$^{VGLUT2+}$::POA neurons
411 may play a role in suppressing anxiety and passive fear behaviors to promote active engagement.
412 Finally, examining the conflicting behaviors required for threat response and feeding we
413 SuM$^{VGLUT2+}$::POA were suppressed during feeding and that activation of SuM$^{VGLUT2+}$::POA
414 neurons blocked feeding activity both during stimulation in the period after stimulation (**Figure 8**).
415 SuM$^{VGLUT2+}$::POA neurons are distinct subset neurons projecting to many but not all areas
416 receiving projections from the total SuM$^{VGLUT2+}$ population. Notably, mHb and DG projections were
417 present in the SuM$^{VGLUT2+}$ population but absent in the SuM$^{VGLUT2+}$::POA projections (**Figure 3K**),
418 consistent with a separation of DG and CA2 projecting SuM neurons (*68*). The extensive
419 arborization of SuM$^{VGLUT2+}$::POA neurons challenges the often-employed neural circuit concept
420 that projection from a single area to a second to mediate or modify a behavior. The projections to
421 PVT, Hb, and PAG are of particular interest because these areas regulate stress coping (*69-72*).
422 Dopamine receptor 2 expressing neurons in the PVT have been implicated in promoting active
423 coping behaviors and may be a potential target of SuM$^{VGLUT2+}$::POA neurons (*8, 9*). The habenula
424 also regulates active vs passive coping behaviors, and the lHb functions in aversive processing
425 making the selective projections of SuM$^{VGLUT2+}$::POA neurons to the lHb of similar interest (*69, 73-*
426 *76*). In addition, the PAG, which receives projections from SuM$^{VGLUT2+}$::POA neurons, has been
427 implicated in regulating defensive behaviors and coping strategies (*70, 71, 77*). The arborization
428 to these and other areas position SuM$^{VGLUT2+}$::POA neurons to be a central hub for regulating
429 behavioral responses to threatening stressors by concurrent recruitment of multiple areas.

430 Superficially, the aversiveness of SuM$^{VGLUT2+}$::POA neuron stimulation we report contrasts
431 with a recent study that found photostimulation of SuM neurons projections could be reinforcing.
432 Photostimulation of projections from SuM to the septum drove place preference (septum) but, the
433 same report found photostimulation of SuM projections in the PVT was aversive(*19*). We report
434 here that SuM$^{VGLUT2+}$::POA neurons also project to the PVT and the septum (**Figure 2**). A plausible
435 interpretation is that SuM contains separable molecularly defined populations of neurons which
436 gate a host of distinct behavioral strategies through their connectivity and or co-transmitter
437 content. Delineating the overarching circuitry will require further studies, but our results together
438 with recent studies establish SuM is an important and poorly understood node for regulating
439 appetitive and aversive motivated behaviors.
440 We addressed the challenge of potential confounds from locomotor activity inherent in
441 active coping behaviors, which is of special concern here because a population of SuM neurons
442 have been found to correlate with velocity of movement, by using multiple behavioral assays with
443 fiber photometry and photostimulation. We found multiple threatening stressors (dunk, shock,
444 ambush) with differing evoked behaviors all recruit SuM$^{VGLUT2+}$::POA neurons (**Figure 3**). We also
445 found increased recruitment of SuM$^{VGLUT2+}$::POA neurons during active coping behaviors
446 (**Figures 3 and 7**). We did not find evidence for recruitment of SuM$^{VGLUT2+}$::POA neurons during
447 elevated locomotion in two cohorts in assays of free movement (**Figure 3K-M and Supplemental**
448 **Figure 5**). These data are in contrast to recent studies that found activity of some neurons in SuM
449 correlated future velocity (*41*). We carefully examined the behaviors elicited by activation of
450 SuM$^{VGLUT2+}$::POA neurons both in absence of stressors (**Figure 4**) and during ongoing stressors
451 (**Figure 7**) and found stimulation of SuM$^{VGLUT2+}$::POA neurons promoted active coping behaviors.
452 Because escape behaviors could be innate fixed behaviors we examined if SuM$^{VGLUT2+}$::POA
453 neurons could also drive performance of an operant task, which would be impaired if activation of
454 SuM$^{VGLUT2+}$::POA neurons lead to fixed escape behaviors. We found mice effectively performed
455 the operant task. In trials using a progressive ratio mice performed the task repetitively during
456 sustained photostimulation because the number of port activations required to terminate the
457 stimulation was high. Taken together the results from the behavioral tests indicate that
458 SuM$^{VGLUT2+}$::POA promote flexible stressor appropriate coping behaviors and not generalized
459 locomotion.
460 Although neurons that release both GABA and glutamate projecting to dentate gyrus are
461 present in SuM, our anatomic studies indicate and SuM$^{VGLUT2+}$::POA neurons were discrete from
462 GABAergic neurons do not project the dentate gyrus (**Figure 2 and Supplemental Figure2**)(*21,*
463 *40*). SuM^{VGAT} could be a functionally distinct population. We tested the effects of photostimulation

464 of SuM^{VGAT} neuron and in contrast to $SuM^{VGLUT2+}$::POA neurons, found no effect on place
465 aversion, minor decreases in locomotion, and no significant change in active coping behaviors
466 during stress (FST) during stimulation. Surprisingly, immediately after photostimulation stopped
467 active coping behavior increased dramatically (**Figure 7I**). These data demonstrate functional
468 separation of SuM^{VGAT} and suggest connection between the $SuM^{VGLUT2+}$::POA and SUM^{VGAT+}
469 populations.

470 The aversiveness of $SuM^{VGLUT2+}$::POA neuron stimulation we report contrasts with a recent
471 study that found photostimulation of SuM neurons projections could be reinforcing. However, mor
472 closer examination suggests the potential underlying diversity of SuM neurons may explain the
473 results. Photostimulation of projections from SuM to the septum drove place preference but
474 photostimulation of SuM projections in the PVT was aversive(*19*). We report here that
475 $SuM^{VGLUT2+}$::POA neurons also project to the PVT and the septum (**Figure 2**). A plausible
476 interpretation is that SuM contains separable populations. One set (PVT projecting) could drive
477 aversion and the other (non-PVT projecting) may regulate reinforcement. Delineating the
478 overarching circuitry will require further studies. Our results together with recent studies establish
479 SuM is an important and poorly understood node for regulating appetitive and aversive motivated
480 behaviors.

481 In conclusion, $SuM^{VGLUT2+}$::POA neurons arborize to multiple areas involved in stress and
482 threat response that promote active coping behaviors. Passive coping strategies have been
483 associated with unescapable stress, anhedonia, and depression(*7, 78-80*). Targeting
484 neuromodulation of a circuit able to act across many brain areas may represent a therapeutic
485 avenue for common psychiatric conditions and $SuM^{VGLUT2+}$::POA neurons are a newly identified
486 node in critical approach-avoidance circuitry.

487 **Acknowledgements**

488 This work was supported by the NIH through 5R01MH112355 to MRB and P30DA048736
489 (MRB) and 5K08MH119538 to AJN. Support was also provided by the Hope Center Viral Vectors
490 Core and the Genome Technology Resource Center at Washington University in St. Louis (NIH
491 P30CA91842 and UL1TR000448). This work was supported by a Pilot Project Award from the
492 Hope Center for Neurological Disorders and by the Hope Center Viral Vectors Core at Washington
493 University School of Medicine.

494

495 **Materials and Methods**

496 **Methods**

497 Key Resources Table:

Reagent type (species) or resource	Source or reference	Identifiers
Antibodies		
Alexa Fluor 488 Goat anti-Rabbit IgG	Invitrogen	Cat# A11008
Phospho-c-Fos (Ser32) (D82C12) XP®	Cell Signaling Technology	Cat# 5348
Chemicals		
4% paraformaldehyde	J.T. Baker, Avantor	S898-09
Goat Serum	Sigma Aldrich	G9023
Vectashield Hardset Antifade Mounting Medium With DAPI	Vector Laboratories	Cat# NC9029229
Experimental Models: Organisms/Strains		
Slc17a6tm2(cre)Lowl/J (VGLUT2-Cre)	The Jackson Laboratory	RRID:IMSR_JAX:016963
B6;129S-Slc17a6tm1.1(flpo)Hze/J (VGLUT2-Flp)	The Jackson Laboratory	RRID: IMSR_JAX: 030212
Mouse:B6.Cg-Gt(ROSA)26Sor$^{tm14(CAG-tdTomato)Hze}$/J (Ai14)	The Jackson Laboratory	RRID: IMSR_JAX: 007914
B6J.129S6(FVB)-*Slc32a1*$^{tm2(cre)Lowl}$/MwarJ (VGAT-Cre)	The Jackson Laboratory	RRID: IMSR_JAX: 028862
C57BL/6J	The Jackson Laboratory	RRID: IMSR_JAX: 000664
Bacterial and Virus Strains		
AAV5-EF1a-DIO-hChR2(H134R)-EYFP (2.5 × 10^{13} vg/ml)	Washington University Hope Center Viral Vector Core	N/A
AAV2-Retro-DIO-ChR2-eYFP (2.8 × 10^{12} vg/ml)	Washington University Hope Center Viral Vector Core	N/A
AAV2-retro-FLEX-tdTomato (7 × 10^{12} vg/ml)	Addgene	RRID: Addgene_28306-AAVrg
AAV5-DIO-ChR2-eYFP (1.4 × 10^{13} vg/ml)	Washington University Hope Center Viral Vector Core	N/A
AAV2-Retro-EF1a-fDIO-cre (7 × 10^{12} vg/ml)	Addgene	RRID: Addgene_121675-AAVrg

AAV2-EF1a-Nuc-flox(mCherry)-EGFP (5 × 10^{12} vg/ml)	Addgene	RRID: Addgene_112677-AAV5
Retro-AAV2-EF1a-Nuc-flox(mCherry)-EGFP	Addgene	RRID: Addgene_ 112677-AAVrg
AAV2-retro-EF1a-DIO-eYFP (3 × 10^{13} vg/ml)	Washington University Hope Center Viral Vector Core	N/A
AAV-retro-EF1a-Flpo (1.02 × 10^{13} GC/mL or 7 × 10^{12} vg/ml)	Addgene	RRID: Addgene_ 55637-AAVrg
AAV9-EF1a-fDIO-cre (2.5 × 10^{13} GC/mL or 1 × 10^{13} vg/ml)	Addgene	RRID: Addgene_121675-AAV9
Retro-AAV2-EF1a-Cre (2.1 × 10^13 GC/mL)	Addgene	RRID: Addgene_55636-AAVrg
AAV9-syn-FLEX-GCaMP7s-WPRE	Addgene	RRID: Addgene_104487-AAV9
Software		
Bonsai	Bonsai-rx.org	N/A
Ethovision	Noldus	N/A
GraphPad Prism	GraphPad Software	N/A

For further information regarding reagents and resources, contact Aaron Norris, norrisa@wustl.edu.

Experimental model and subject details

Adult (25-35 g, at least 8 weeks of age upon experimental use) male and female VGLUT-Cre (RRID: IMSR_JAX:016963), VGLUT2-Flp (RRID: IMSR_JAX: 030212), Ai14 (RRID: IMSR_JAX: 007908), VGAT-Cre (RRID: IMSR_ JAX: 028862) and C57BL/6J (RRID: IMSR_JAX: 000664) mice (species *Mus musculus*) were group housed (no more than five littermates per cage) in a 12 hr:12 hr light:dark cycle room with food and water ad libitum(*81*). The Washington University Animal Care and Use Committee approved all procedures which adhered to NIH guidelines.

510 Stereotaxic surgery

511 Injections and implantations were done as described previously(*34, 82*). Briefly, in an
512 induction chamber, mice were anesthetized (4% isoflurane) before being placed in a stereotaxic
513 frame (Kopf Instruments). Anesthesia was maintained with 2% isoflurane. Mice were then injected
514 unilaterally or bilaterally, depending on the combination of virus(es) used and brain regions
515 injected. A blunt needle Neuros Syringe (65457-01, Hamilton Con.) and syringe pump (World
516 Precision Instruments) were used to perform the injection schemes below. After surgery, a
517 warmed recovery chamber housed the animal while it recovered from anesthesia before being
518 returned to its home cage.

Virus	Virus Volume	Brain region/coordinates
AAV5-EF1a-DIO-hChR2(H134R)-EYFP	100 nl	Region, laterality, (AP , ML , DV)
AAV2-retro-DIO-ChR2-eYFP	100 nl	SuM (AP -2.7, ML +0.05, DV -4.3)
AAV2-retro-FLEX-tdTomato	100 nl	Septum (AP +0.9, ML +0.3, DV -3.5) LPAG, unilateral (AP -4.65, ML +0.6, DV -2.85)
AAV2-retro-EF1a-fDIO-cre	100 nl	POA, bilateral (AP +0.45, ML ± 0.5, DV -5.35)
AAV2-EF1a-Nuc-flox(mCherry)-EGFP	300 nl	SuM (AP -2.7, ML +0.05, DV -4.3)
AAV2-retro-EF1a-Nuc-flox(mCherry)-EGFP	150 nl	POA, bilateral (AP +0.45, ML ± 0.5, DV -5.35)
AAV22-retro-EF1a-DIO-eYFP	100 nl	Acb (AP +1.4, +0.6 ML, DV -4.75) POA, bilateral (AP +0.45, ML ± 0.5, DV -5.35)
AAV2-retro-EF1a-Flpo	50 nl	POA, bilateral (AP +0.45, ML ± 0.5, DV -5.35)
AAV9-EF1a-fDIO-cre	100 nl or 50 nl	SuM m(AP -2.7, ML +0.05, DV -4.3)

519 Injections were made at a rate of 50 nl/min, with the injection needle being withdrawn 5
520 min after the end of the infusion. Fiber optics for photostimulation or optical fibers for fiber
521 photometry were implanted after injections for all behavioral experiments. Fiber optics for
522 photostimulation or optical fibers for fiber photometry were implanted after injections for all
523 behavioral experiments.

524 Fiber optic implants for photostimulation were fabricated as previously described using
525 200µm glass fibers and implanted midline over SuM (*34, 83*). For implantation, the skull was
526 cleaned and etched with OptiBond® (Kerr) and the fiber was cemented to the skull with Tetric N-
527 Flow® (Ivoclar Vivadent). Blue light was used to cure and harden cement. Mice were allowed to
528 recover for at least seven days before the start of behavioral experiments. The same process was

529 used for implantation for fiber photometry fibers, which were trimmed to length
530 (NeuroPhotometrics).
531 Anatomical tracing
532 For anterograde viral tracing experiments, virus (was injected at least six weeks prior to
533 transcardial perfusions with 4% paraformaldehyde to allow for anterograde transport of the
534 fluorophore. AAV5-EF1a-DIO-hChR2eYFP or AAV5-EF1a-DIO-eYFP were used. Alternatively, to
535 label only $SuM^{VGLUT2+}$::POA neurons for anterograde tracing Retro-AAV2-DIO-eYFP or Retro-
536 DIO-ChR21eYFP was injected into the POA with AAV-fDIO-Cre injected in the SuM. A minimum
537 of 6 weeks was allowed prior to sacrifice, harvesting or brains, and sectioning (30μM). Serial 30
538 μM sections approximately 60μM apart were examined. For retrograde studies viruses were
539 injected (see figure legends and text for specific viruses) at the targeted site and table for specific
540 viruses(*84-86*). Three weeks were allowed to elapse prior to harvesting brains following injections.
541 Images were obtained on a Leica DM6 B upright microscope and processed using Thunder
542 imaging station (Leica).
543 Brain clearing and light sheet microscopy
544 Tissue clearing and imaging was carried out on brains collected and fixed in 4% PFA as
545 described above by LifeCanvas Technologies. Briefly, brains were fixed using SHIELD post ix
546 and cleared for 7 days in SmartClear II Pro. Index matched with EASYIndex at room temperature.
547 Samples were mounted ventral side up and imaged at 3.6x with pixel size 1.8 x 1.8 mm, axial
548 resolution < 4 μm, z step 4 μm in 488nm channel. Fos was labeled by Alexa Flour 488. SuM
549 boundaries were defined by -2.6 to -2.95 rostral to Bregma. The medial mammillary nucleus and
550 the mammillary recess of the 3rd ventricle marked the medial and ventral boundaries while fornix
551 marked the lateral, and fasciculus retroflexus the dorsal boundaries. Images were quantified by a
552 trained laboratory member who was blind to the experimental conditions.
553 Immunohistochemistry
554 Mice were intracardially perfused with 4% PFA and then brains were sectioned (30
555 microns) and placed in 1x PB until immunostaining. Free-floating sections were washed in 3 times
556 in 1x PBS for 10 min intervals. Sections were then placed in blocking buffer (0.5% Triton X-100%
557 and 5% natural goat serum in 1z PBS) for 1 hr at room temperature. After blocking buffer, sections
558 were placed in primary antibody rabbit Phospho-c-Fos (Ser32) antibody (1:500, Cell Signaling
559 Technology) overnight 4° C temperature. After 3 x 10 min 1x PBS washes, sections were
560 incubated in secondary antibody goat anti-rabbit Alexa Fluor 488 (1:2500, Invitrogen) for 2 hr at
561 room temperature. Sections were washed in 1x PBS (3 x 10 min) followed by 2 x 10 min 1x PB
562 washes. After immunostaining, sections were mounted on Super Frost Plus slides (Fisher) and

563 covered with Vectashield Hard set mounting medium with DAPI (RRID:AB_2336788, Vector
564 Laboratories) and cover glass prior to being imaged.

565 Imaging and cell quantification

566 'The Mouse Brain in Stereotaxic Coordinates' provided the framework to label brain
567 sections relative to bregma(*87*). A Leica DM6 B epifluorescent microscope was used to image all
568 sections. For eYFP visualization, a YFP filter cube (Excitation: 490-510, Dichroic: 515, Emission:
569 520-550) was used and for tdTomato visualization, a Texas Red Filter Cube (Excitation: BP
570 560/40, Dichroic: LP 585, Emission: BP 630/75) was used. Fos was labeled by Alexa Flour 488.
571 SuM boundaries were defined by -2.6 to -2.95 rostral to Bregma. The medial mammillary nucleus
572 and the mammillary recess of the 3rd ventricle marked the medial and ventral boundaries while
573 fornix marked the lateral, and fasciculus retroflexus the dorsal boundaries. Images were quantified
574 by a trained laboratory member who was blind to the experimental conditions.

575 Forced-Swim Test

576 For stress induction via forced swim (**Figure 4**)(*65, 88*), mice were individually placed in
577 a cylindrical container (18 cm in diameter) filled with water at 25 +/- 1 ^{o}C for 15 min. Prior to stress
578 force swimming, mice were habituated to the arenas for three days prior to the beginning of FST
579 to minimize stress. Control mice were brought to the behavioral testing area but remained in the
580 home cage until sacrifice. Water was replaced after every animal.

581 Fiber Photometry

582 For all fiber photometry experiments the same strategy to selectively label
583 SuM$^{VGLUT2+}$::POA neurons was used. VGLUT2-Flp mice were injected bilaterally in POA with AAV-
584 Retro-EF1a-fDIO-Cre and with AAV-syn-FLEX-GCaMP7s-WPRE in SuM. After two weeks, mice
585 were implanted with fiber-optic cannulas (200µm) in SuM (D/V -4.3-5)(*89*). Mice recovered a
586 minimum of one week prior to behavioral testing. Recording of Ca^{2+} dependent and isosbestic
587 signals were obtained using previous described methods with Bonsai software and FP3002
588 (Neurophotometrics)(*63, 90*). 470 and 415 nm LEDs were used to record interleaved isosbestic
589 and Ca^{2+} dependent signals following the manufacturer directions.

590 For repeated forced swim experiments (dunk tank) mice were placed inside a custom-
591 made plastic rectangular enclosure (20 cm x 20cm x 23 cm) filled with water 30 +/- 1 ^{o}C. The
592 enclosure has a square wire mesh platform that could be raised and lowered without touching the
593 animal. The platform was lowered for the swim session and raised at the conclusion of each
594 session. During testing mice were tethered to a fiberoptic patch cabled that was attached to a
595 counter balanced arm that prevented downward force on the animal. Time mobile was quantified
596 by a trained observer for the ten 30s trials.

597 For foot shock stress testing, mice were individually placed inside a custom-made clear
598 plastic box (15.24 L x 13.34 W x 14 H cm) inside a sound-attenuated cabinet. A speaker was
599 placed 4 cm above the chamber for the delivery of auditory cues (75dB). A constant current
600 aversive stimulator (ENV-414S) delivered foot shocks through a grid floor (0.7mA). Five shocks
601 of 2 sec were delivered after a 30 s tone. Intertrial interval ranged from 90 to 180 sec. After the
602 session, the animal was removed from the chamber and placed back in its home cage. The
603 chamber and grid were wiped down with 70% ethanol between animals.
604 For open field testing for velocity measurements, mice were tethered to a fiberoptic patch
605 cable and placed inside a custom-built square arena (50.8 cm x 50.8 cm x 50.8 cm). Mice were
606 allowed to explore the arena for a 20 min session. Velocity was quantified using scripts in Bonsai
607 2.4. Bedding in the arena was replaced between animals, and the floors and walls of the arena
608 were wiped down with 70% ethanol.
609 Similar to the repeated forced swim experiments, for forced swim mice were placed on top
610 of a square wire mesh platform that could be raised and lowered inside a custom-made plastic
611 rectangular enclosure (20 cm x 20 cm x 23 cm) filled with water at 25 +/- 1 ºC. The platform was
612 lowered at the beginning of the test for 15 min and raised at the conclusion of the test. During
613 testing, mice were tethered to a fiberoptic patch cable that was attached to a counter balanced
614 arm that prevented downward force on the animal. Water was replaced between animals and the
615 enclosure was wiped down with 70% ethanol and rinsed with water. Time immobile, hindpaw
616 swim, swimming, and climbing were quantified using LabGym (Hu et al., 2022).
617 To test the response to a natural stressor that mice can potentially encounter in their
618 natural habitat(*91*). in $SuM^{VGLUT2+}$::POA neurons, a remote-controlled spider was used to simulate
619 an ambush of a potential predator. The remote-controlled spider (17 cm x 16 cm; Amazon) was
620 placed inside a polylactic acid (PLA) enclosure (19 cm x 20 cm x 23 cm) that was then placed
621 inside a custom-built square arena (50.8 cm x 50.8 cm x 50.8 cm). Mice were tethered to a
622 fiberoptic patch cable and placed inside the arena for 10 min. Baseline activity was recorded for
623 5 min before the ambush. After 5 min, the animal was ambushed once it moved in close proximity
624 to the spider's enclosure (Supplemental video 4). Velocity was measured and analyzed using
625 DeepLabCut (Mathis et al., 2019) within Bonsai. The arena and spider's enclosure were wiped
626 down with 70% ethanol between animals.
627 For experiments that examined recruitment of $SuM^{VGLUT2+}$::POA neurons during
628 consummatory behavior, mice were food deprived or given adlib access to food for 24 hours prior
629 to testing. On test day, mice were placed inside an 18 cm diameter round arena and allowed to
630 habituate for 30 min before they were tethered to the fiberoptic path cable. Once tethered, mice

631 were placed inside the arena for 20 min. Baseline activity was recorded for 5 min before the
632 introduction of the chow pellet and for 15 min after the chow pellet was introduced. Chow pellets
633 were weighed before and after the 20-min trial. The difference is reported as food eaten. The
634 same procedure was followed for control mice with the only difference being that these animals
635 were not food deprived for 24 hours.

636 For fiber photometry data analysis, the interleaved isosbestic and Ca^{2+} dependent signals
637 were recorded at 60 fps (30 fps each). Deinterleaved signals were analyzed using methods as
638 previously reported (*90*). Briefly, raw signals were smoothed using a moving average, fitted with
639 an exponential curve using a non-linear least squares function for baseline correction, signals
640 were standardized using the mean value and standard deviation (Z-Score), the standardized
641 isosbestic and Ca2+ signals were scaled a non-negative robust linear regression, and normalized
642 dF/F was calculated. In experiments shown in figures 7A and 8 E-F there was sustained step drop
643 evident in the Ca^{2+} dependent signal reflecting change in population activity because it was not
644 seen in the isosbestic signal. The nature and duration of the change of the signal precluded fitting
645 a curve to the Ca^{2+} dependent signal. In these cases, we show both the Ca^{2+} dependent and
646 isosbestic signals. Z-scores were calculated without baseline correction for both Ca^{2+} dependent
647 and isosbestic signals based on the variability in the baseline state.

648

649 <u>Real-time place aversion testing</u>

650 For real-time place preference testing with optogenetic photostimulation we used custom-
651 made, unbiased, balanced two-compartment conditioning apparatus (52.5 x 25.5 x 25.5 cm) as
652 described previously(*34, 82, 92*). Mice were tethered to a patch cable that allowed free access to
653 the entire arena for 30 min. Entry into one compartment triggered photostimulation, 1Hz, 5Hz,
654 10Hz, or 20 Hz (473 nm laser, 10 ms pulse width) that persisted while the mouse remained in the
655 light paired side. The side paired with photostimulation was counterbalanced across mice.
656 Ordering was counterbalanced with respect to stimulation frequency and placement. Bedding in
657 the behavior apparatus was replaced between every trial, and the floors and walls of the
658 apparatus were wiped down with 70% ethanol. Time spent in each chamber and total distance
659 traveled for the entire 30-min trial was measured using Ethovision 10 (Noldus Information
660 Technologies).

661 <u>Light /Dark choice</u>

662 For light/dark choice the same areas as used for real time preference testing were
663 modified and used as previously described (*93*). On the light side a small sport light was placed
664 overhead, and the walls were covered with white laminated paper. Light levels on this side

665 measure 580-590 lux. For the dark side, an infrared spotlight was placed over head, to allow for
666 video tracking of the mice. The walls were covered with matte black plastic. Light levels in the
667 center of the dark side measure 100-110 lux. Animals were recorded using a USB web cam
668 without an infrared filter. For real-time aversion testing photostimulation was paired with the dark
669 side of arena as described above. For anxiety-like behavior testing stimulation was provided
670 uniformly during the trials. Time spent in each chamber and total distance traveled for the entire
671 30-min trial was measured using Ethovision 10.

672 Observational behavioral assay

673 To observe behaviors evoked by photostimulation of $SuM^{VGLUT2+}$::POA neurons we mice
674 were habituated for at least 3 days prior to testing to round (18 cm diameter) clear arena with
675 counterbalanced optical commutators to minimize impact of the head tether on movement.
676 Testing occurred after habitation and approximately 2 cm of bedding material was placed in the
677 arena. Behavior was recorded from the side and scored by a blinded observer.

678 Negative reinforcer two nose port operant behavior testing

679 For operant behavior testing we used Med Associates mouse operant conditioning
680 chamber with dual nose ports and house light as previously described(*63*). Briefly, mice were
681 tethered via cantilevered counterweighted optical commutator to a laser light source. A five-day
682 protocol call was used. Day one through four were 10-min trials. Photostimulation was provided
683 at 10 Hz and activation of the active port resulted in a 10-second pause in the photostimulation
684 and activation of the house light inside the arena. On the first four days each activation of the
685 active port outside of a 10-second pause resulted in a new pause. On day five was a 30-min trial
686 using a progressive ratio protocol the number activation of the active port to generate a pause
687 increased with each activation based on the $number\ of\ activations\ (j) = [5e^{(0.2j)} - 5]$ round to
688 the nearest integer generating the schedule 1, 2, 4, 6, 9, 12, 15, 20, 25, 32, 40, 50….(*94*). The
689 trial was limited to 30-mins due to concern for animal welfare due to the head tether and confined
690 space. Photostimulation terminated at the conclusion of the trial.

691 Forced Swim with photostimulation

692 Forced swim trials with optogenetic stimulation were done as a two-day test. On the first
693 day all mice were subjected to a 15-min forced swim, dried and returned to the home cage. On
694 the second day they were tethered and subjected to a 6-min forced swim divided into three
695 periods, each two mins in length, pre stimulation, stimulation, and post stimulation. 10 Hz
696 photostimulation was provided during the trial. Mice were closely monitored during each trial of
697 swimming. Trials were recorded and scored by a blinded observer for time spent immobile on the
698 second day of the test.

Feeding after food deprivation

For tests involving brief access to food after deprivation, the same 18 cm diameter round arenas with counterbalanced optical commutators were used. Mice were habituated to the arenas for a minimum 3 days prior to testing. Mice were food deprived by removal of food from the home cage 24 hours prior to testing. Mice were placed in the arena and allowed to habituate prior to introduction of a chow pellet. The 20-minutue trial with the foot pellet was recorded and scored by a blinded observer. Chow pellets were weighed before and after the 20-min trial. The difference is reported as food eaten.

Open Field Test

For Open Field testing we used a purpose-built 20in square behavior arena. Mice were tethered to a patch cable and placed into the behavioral arena. The laser frequency was set to 10 Hz and was left on for 20 mins. Distance moved for the 20-min trial was quantified using Ethovision 10. Bedding in the arena was replaced between every trial, and the floors and walls of the arena were wiped down with 70% ethanol.

Statistical analyses

Statistical analyses were conducted using GraphPad Prism software. Data are shown as mean ±SEM except for z-scores which as shown as ± 95% confidence interval, as noted in text. Values for individual p values are given in the text and figure legends. Significance was held at α less than 0.05. Unless noted in the test, nonparametric Mann-Whitney tests were used for statistical comparisons. In cases of multiple comparisons, Holm-Šídák method was used to correct for multiple comparisons. Paired testing was used with comparing within cohorts with repeated measurements and unpaired between cohorts. All “n” values represent the number of animals in a particular group for an experiment. For fiber photometry statistical analysis, the mean signal of the baseline and stimulus windows was used, and comparisons were made using the Wilcoxon ranked-sum test, with α=0.95.

Citations

1. J. LeDoux, N. D. Daw, Surviving threats: neural circuit and computational implications of a new taxonomy of defensive behaviour. *Nat Rev Neurosci* **19**, 269-282 (2018).
2. J. E. LeDoux, Coming to terms with fear. *Proc Natl Acad Sci U S A* **111**, 2871-2878 (2014).
3. D. Mobbs, C. C. Hagan, T. Dalgleish, B. Silston, C. Prevost, The ecology of human fear: survival optimization and the nervous system. *Front Neurosci* **9**, 55 (2015).
4. L. M. Shin, I. Liberzon, The neurocircuitry of fear, stress, and anxiety disorders. *Neuropsychopharmacology* **35**, 169-191 (2010).
5. K. J. Ressler, H. S. Mayberg, Targeting abnormal neural circuits in mood and anxiety disorders: from the laboratory to the clinic. *Nat Neurosci* **10**, 1116-1124 (2007).
6. R. C. Kessler *et al.*, Lifetime prevalence and age-of-onset distributions of mental disorders in the World Health Organization's World Mental Health Survey Initiative. *World Psychiatry* **6**, 168-176 (2007).
7. S. M. Southwick, M. Vythilingam, D. S. J. A. R. C. P. Charney, The psychobiology of depression and resilience to stress: implications for prevention and treatment. **1**, 255-291 (2005).
8. M. A. Penzo *et al.*, The paraventricular thalamus controls a central amygdala fear circuit. *Nature* **519**, 455-459 (2015).
9. J. Ma *et al.*, Divergent projections of the paraventricular nucleus of the thalamus mediate the selection of passive and active defensive behaviors. *Nat Neurosci* **24**, 1429-1440 (2021).
10. J. E. Ledoux, J. M. Gorman, A call to action: Overcoming anxiety through active coping. *Am J Psychiat* **158**, 1953-1955 (2001).
11. T. Steimer, Animal models of anxiety disorders in rats and mice: some conceptual issues. *Dialogues Clin Neurosci* **13**, 495-506 (2011).
12. C. T. Gross, N. S. Canteras, The many paths to fear. *Nat Rev Neurosci* **13**, 651-658 (2012).
13. P. Amorapanth, J. E. LeDoux, K. Nader, Different lateral amygdala outputs mediate reactions and actions elicited by a fear-arousing stimulus. *Nat Neurosci* **3**, 74-79 (2000).
14. N. S. Canteras, S. Chiavegatto, L. E. Ribeiro do Valle, L. W. Swanson, Severe reduction of rat defensive behavior to a predator by discrete hypothalamic chemical lesions. *Brain Res Bull* **44**, 297-305 (1997).
15. W. X. Pan, N. McNaughton, The supramammillary area: its organization, functions and relationship to the hippocampus. *Prog Neurobiol* **74**, 127-166 (2004).
16. R. P. Vertes, J. T. McKenna, Collateral projections from the supramammillary nucleus to the medial septum and hippocampus. *Synapse* **38**, 281-293 (2000).
17. R. P. Vertes, Pha-L Analysis of Projections from the Supramammillary Nucleus in the Rat. *J Comp Neurol* **326**, 595-622 (1992).
18. J. Kiss, A. Csaki, H. Bokor, K. Kocsis, B. Kocsis, Possible glutamatergic/aspartatergic projections to the supramammillary nucleus and their origins in the rat studied by selective [(3)H]D-aspartate labelling and immunocytochemistry. *Neuroscience* **111**, 671-691 (2002).
19. A. J. Kesner *et al.*, Supramammillary neurons projecting to the septum regulate dopamine and motivation for environmental interaction in mice. *Nat Commun* **12**, 2811 (2021).
20. Y. Li *et al.*, Supramammillary nucleus synchronizes with dentate gyrus to regulate spatial memory retrieval through glutamate release. *Elife* **9**, (2020).
21. F. Billwiller *et al.*, GABA-glutamate supramammillary neurons control theta and gamma oscillations in the dentate gyrus during paradoxical (REM) sleep. *Brain Struct Funct* **225**, 2643-2668 (2020).

22. H. T. Ito, E. I. Moser, M. B. Moser, Supramammillary Nucleus Modulates Spike-Time Coordination in the Prefrontal-Thalamo-Hippocampal Circuit during Navigation. *Neuron* **99**, 576-587 e575 (2018).
23. N. P. Pedersen *et al.*, Supramammillary glutamate neurons are a key node of the arousal system. *Nat Commun* **8**, (2017).
24. C. Leranth, J. Kiss, A population of supramammillary area calretinin neurons terminating on medial septal area cholinergic and lateral septal area calbindin-containing cells are aspartate/glutamatergic. *J Neurosci* **16**, 7699-7710 (1996).
25. L. J. B. r. b. Swanson, The projections of the ventral tegmental area and adjacent regions: a combined fluorescent retrograde tracer and immunofluorescence study in the rat. **9**, 321-353 (1982).
26. K. Kocsis, J. Kiss, A. Csaki, B. Halasz, Location of putative glutamatergic neurons projecting to the medial preoptic area of the rat hypothalamus. *Brain Res Bull* **61**, 459-468 (2003).
27. W.-X. Pan, N. J. P. i. n. McNaughton, The supramammillary area: its organization, functions and relationship to the hippocampus. **74**, 127-166 (2004).
28. R. Soussi, N. Zhang, S. Tahtakran, C. R. Houser, M. J. E. J. o. N. Esclapez, Heterogeneity of the supramammillary–hippocampal pathways: Evidence for a unique GABAergic neurotransmitter phenotype and regional differences. **32**, 771-785 (2010).
29. S. L. Reitz, A. Z. Wasilczuk, G. H. Beh, A. Proekt, M. B. Kelz, Activation of Preoptic Tachykinin 1 Neurons Promotes Wakefulness over Sleep and Volatile Anesthetic-Induced Unconsciousness. *Curr Biol* **31**, 394-405 e394 (2021).
30. T. Yamagata *et al.*, The hypothalamic link between arousal and sleep homeostasis in mice. *Proc Natl Acad Sci U S A* **118**, (2021).
31. R. Szymusiak, N. Alam, T. L. Steininger, D. McGinty, Sleep-waking discharge patterns of ventrolateral preoptic/anterior hypothalamic neurons in rats. *Brain Res* **803**, 178-188 (1998).
32. M. Nollet, W. Wisden, N. P. Franks, Sleep deprivation and stress: a reciprocal relationship. *Interface Focus* **10**, 20190092 (2020).
33. D. McGinty, R. Szymusiak, Hypothalamic regulation of sleep and arousal. *Front Biosci* **8**, s1074-1083 (2003).
34. A. J. Norris, J. R. Shaker, A. L. Cone, I. B. Ndiokho, M. R. Bruchas, Parabrachial opioidergic projections to preoptic hypothalamus mediate behavioral and physiological thermal defenses. *Elife* **10**, (2021).
35. D. J. Barker *et al.*, Lateral Preoptic Control of the Lateral Habenula through Convergent Glutamate and GABA Transmission. *Cell Rep* **21**, 1757-1769 (2017).
36. K. Nakamura, Y. Nakamura, N. Kataoka, A hypothalamomedullary network for physiological responses to environmental stresses. *Nat Rev Neurosci* **23**, 35-52 (2022).
37. G. W. Zhang *et al.*, Medial preoptic area antagonistically mediates stress-induced anxiety and parental behavior. *Nat Neurosci* **24**, 516-528 (2021).
38. L. Haglund, L. W. Swanson, C. Kohler, The Projection of the Supramammillary Nucleus to the Hippocampal-Formation - an Immunohistochemical and Anterograde Transport Study with the Lectin Pha-L in the Rat. *J Comp Neurol* **229**, 171-185 (1984).
39. T. Hayakawa, H. Ito, K. Zyo, Neuroanatomical Study of Afferent-Projections to the Supramammillary Nucleus of the Rat. *Anat Embryol* **188**, 139-148 (1993).
40. Y. Hashimotodani, F. Karube, Y. Yanagawa, F. Fujiyama, M. Kano, Supramammillary Nucleus Afferents to the Dentate Gyrus Co-release Glutamate and GABA and Potentiate Granule Cell Output. *Cell Rep* **25**, 2704-2715 e2704 (2018).
41. J. S. Farrell *et al.*, Supramammillary regulation of locomotion and hippocampal activity. *Science* **374**, 1492-1496 (2021).

42. Y. G. Park *et al.*, Protection of tissue physicochemical properties using polyfunctional crosslinkers. *Nat Biotechnol*, (2018).
43. L. Madisen *et al.*, A robust and high-throughput Cre reporting and characterization system for the whole mouse brain. *Nat Neurosci* **13**, 133-140 (2010).
44. H. E. Day, C. V. Masini, S. Campeau, The pattern of brain c-fos mRNA induced by a component of fox odor, 2,5-dihydro-2,4,5-trimethylthiazoline (TMT), in rats, suggests both systemic and processive stress characteristics. *Brain Res* **1025**, 139-151 (2004).
45. L. J. Santin *et al.*, c-Fos expression in supramammillary and medial mammillary nuclei following spatial reference and working memory tasks. *Physiol Behav* **78**, 733-739 (2003).
46. E. P. Azevedo *et al.*, A limbic circuit selectively links active escape to food suppression. *eLife* **9**, e58894 (2020).
47. S. F. De Boer, J. M. Koolhaas, Defensive burying in rodents: ethology, neurobiology and psychopharmacology. *Eur J Pharmacol* **463**, 145-161 (2003).
48. D. C. Castro, R. A. Terry, K. C. Berridge, Orexin in Rostral Hotspot of Nucleus Accumbens Enhances Sucrose 'Liking' and Intake but Scopolamine in Caudal Shell Shifts 'Liking' Toward 'Disgust' and 'Fear'. *Neuropsychopharmacology* **41**, 2101-2111 (2016).
49. S. M. Reynolds, K. C. Berridge, Fear and feeding in the nucleus accumbens shell: rostrocaudal segregation of GABA-elicited defensive behavior versus eating behavior. *J Neurosci* **21**, 3261-3270 (2001).
50. J. M. Richard, K. C. Berridge, Nucleus accumbens dopamine/glutamate interaction switches modes to generate desire versus dread: D(1) alone for appetitive eating but D(1) and D(2) together for fear. *J Neurosci* **31**, 12866-12879 (2011).
51. A. V. Kalueff, P. J. B. R. P. Tuohimaa, Grooming analysis algorithm for neurobehavioural stress research. **13**, 151-158 (2004).
52. A. M. van Erp, M. R. Kruk, W. Meelis, D. C. Willekens-Bramer, Effect of environmental stressors on time course, variability and form of self-grooming in the rat: handling, social contact, defeat, novelty, restraint and fur moistening. *Behav Brain Res* **65**, 47-55 (1994).
53. A. V. Kravitz, L. D. Tye, A. C. Kreitzer, Distinct roles for direct and indirect pathway striatal neurons in reinforcement. *Nat Neurosci* **15**, 816-818 (2012).
54. J. G. McCall *et al.*, CRH Engagement of the Locus Coeruleus Noradrenergic System Mediates Stress-Induced Anxiety. *Neuron* **87**, 605-620 (2015).
55. A. C. Felix-Ortiz *et al.*, BLA to vHPC inputs modulate anxiety-related behaviors. *Neuron* **79**, 658-664 (2013).
56. M. Jakovcevski, M. Schachner, F. Morellini, Susceptibility to the long-term anxiogenic effects of an acute stressor is mediated by the activation of the glucocorticoid receptors. *Neuropharmacology* **61**, 1297-1305 (2011).
57. K. R. Bailey, J. N. Crawley, in *Methods of Behavior Analysis in Neuroscience,* nd, J. J. Buccafusco, Eds. (Boca Raton (FL), 2009).
58. L. Heredia, M. Torrente, M. T. Colomina, J. L. J. J. o. p. Domingo, t. methods, Assessing anxiety in C57BL/6J mice: a pharmacological characterization of the open-field and light/dark tests. **69**, 108-114 (2014).
59. L. Prut, C. J. E. j. o. p. Belzung, The open field as a paradigm to measure the effects of drugs on anxiety-like behaviors: a review. **463**, 3-33 (2003).
60. F. Chaouloff, M. Durand, P. J. B. b. r. Mormède, Anxiety-and activity-related effects of diazepam and chlordiazepoxide in the rat light/dark and dark/light tests. **85**, 27-35 (1997).
61. D. Mobbs, C. C. Hagan, T. Dalgleish, B. Silston, C. J. F. i. n. Prévost, The ecology of human fear: survival optimization and the nervous system. **9**, 55 (2015).

863 62. J. P. Fadok *et al.*, A competitive inhibitory circuit for selection of active and passive fear responses.
864 *Nature* **542**, 96-100 (2017).
865 63. K. E. Parker *et al.*, A Paranigral VTA Nociceptin Circuit that Constrains Motivation for Reward. *Cell*
866 **178**, 653-671 e619 (2019).
867 64. A. P. Costa *et al.*, A proposal for refining the forced swim test in Swiss mice. *Prog*
868 *Neuropsychopharmacol Biol Psychiatry* **45**, 150-155 (2013).
869 65. K. G. Commons, A. B. Cholanians, J. A. Babb, D. G. Ehlinger, The Rodent Forced Swim Test
870 Measures Stress-Coping Strategy, Not Depression-like Behavior. *ACS Chem Neurosci* **8**, 955-960
871 (2017).
872 66. Y. Hu *et al.*, LabGym: quantification of user-defined animal behaviors using learning-
873 based holistic assessment. 2022.2002.2017.480911 (2022).
874 67. C. Seo *et al.*, Intense threat switches dorsal raphe serotonin neurons to a paradoxical operational
875 mode. **363**, 538-542 (2019).
876 68. S. Chen *et al.*, A hypothalamic novelty signal modulates hippocampal memory. *Nature* **586**, 270-
877 274 (2020).
878 69. A. S. Andalman *et al.*, Neuronal Dynamics Regulating Brain and Behavioral State Transitions. *Cell*
879 **177**, 970-985 e920 (2019).
880 70. O. Berton *et al.*, Induction of deltaFosB in the periaqueductal gray by stress promotes active
881 coping responses. *Neuron* **55**, 289-300 (2007).
882 71. P. Tovote *et al.*, Midbrain circuits for defensive behaviour. *Nature* **534**, 206-212 (2016).
883 72. K. A. Keay, R. Bandler, Parallel circuits mediating distinct emotional coping reactions to different
884 types of stress. *Neurosci Biobehav Rev* **25**, 669-678 (2001).
885 73. A. Lee *et al.*, The habenula prevents helpless behavior in larval zebrafish. *Curr Biol* **20**, 2211-2216
886 (2010).
887 74. B. Li *et al.*, Synaptic potentiation onto habenula neurons in the learned helplessness model of
888 depression. *Nature* **470**, 535-539 (2011).
889 75. I. Lazaridis *et al.*, A hypothalamus-habenula circuit controls aversion. **24**, 1351-1368 (2019).
890 76. S. Mondoloni, M. Mameli, M. J. T. P. Congiu, Reward and aversion encoding in the lateral habenula
891 for innate and learned behaviours. **12**, 3 (2022).
892 77. K. A. Keay, R. Bandler, Parallel circuits mediating distinct emotional coping reactions to different
893 types of stress. *Neurosci Biobehav R* **25**, 669-678 (2001).
894 78. J. F. Cryan, R. J. Valentino, I. Lucki, Assessing substrates underlying the behavioral effects of
895 antidepressants using the modified rat forced swimming test. *Neurosci Biobehav Rev* **29**, 547-569
896 (2005).
897 79. A. T. Knoll, W. A. J. B. r. Carlezon Jr, Dynorphin, stress, and depression. **1314**, 56-73 (2010).
898 80. K. Ebner, N. J. C. O. i. B. S. Singewald, Individual differences in stress susceptibility and stress
899 inhibitory mechanisms. **14**, 54-64 (2017).
900 81. L. Vong *et al.*, Leptin action on GABAergic neurons prevents obesity and reduces inhibitory tone
901 to POMC neurons. *Neuron* **71**, 142-154 (2011).
902 82. J. G. McCall *et al.*, CRH Engagement of the Locus Coeruleus Noradrenergic System Mediates
903 Stress-Induced Anxiety. *Neuron* **87**, 605-620 (2015).
904 83. D. R. Sparta *et al.*, Construction of implantable optical fibers for long-term optogenetic
905 manipulation of neural circuits. *Nat Protoc* **7**, 12-23 (2011).
906 84. L. E. Fenno *et al.*, Targeting cells with single vectors using multiple-feature Boolean logic. *Nat*
907 *Methods* **11**, 763-772 (2014).
908 85. S. Back *et al.*, Neuron-Specific Genome Modification in the Adult Rat Brain Using CRISPR-Cas9
909 Transgenic Rats. *Neuron* **102**, 105-119 e108 (2019).

910 86. J. H. Lee *et al.*, Global and local fMRI signals driven by neurons defined optogenetically by type
911 and wiring. *Nature* **465**, 788-792 (2010).
912 87. G. Paxinos, K. B. Franklin, *Paxinos and Franklin's the mouse brain in stereotaxic coordinates*.
913 (Academic press, 2019).
914 88. R. D. Porsolt, A. Bertin, N. Blavet, M. Deniel, M. Jalfre, Immobility induced by forced swimming in
915 rats: effects of agents which modify central catecholamine and serotonin activity. *Eur J Pharmacol*
916 **57**, 201-210 (1979).
917 89. H. Dana *et al.*, High-performance calcium sensors for imaging activity in neuronal populations and
918 microcompartments. *Nat Methods* **16**, 649-657 (2019).
919 90. E. Martianova, S. Aronson, C. D. Proulx, Multi-Fiber Photometry to Record Neural Activity in
920 Freely-Moving Animals. *J Vis Exp*, (2019).
921 91. M. Nyffeler, R. S. Vetter, Black widow spiders, Latrodectus spp. (Araneae:
922 Theridiidae), and other spiders feeding on mammals. *The Journal of Arachnology* **46**, 541-548
923 (2018).
924 92. A. M. Stamatakis, G. D. Stuber, Activation of lateral habenula inputs to the ventral midbrain
925 promotes behavioral avoidance. *Nat Neurosci* **15**, 1105-1107 (2012).
926 93. A. T. Luskin *et al.*, Extended amygdala-parabrachial circuits alter threat assessment and regulate
927 feeding. *Sci Adv* **7**, (2021).
928 94. N. R. Richardson, D. C. Roberts, Progressive ratio schedules in drug self-administration studies in
929 rats: a method to evaluate reinforcing efficacy. *J Neurosci Methods* **66**, 1-11 (1996).

Figure 1

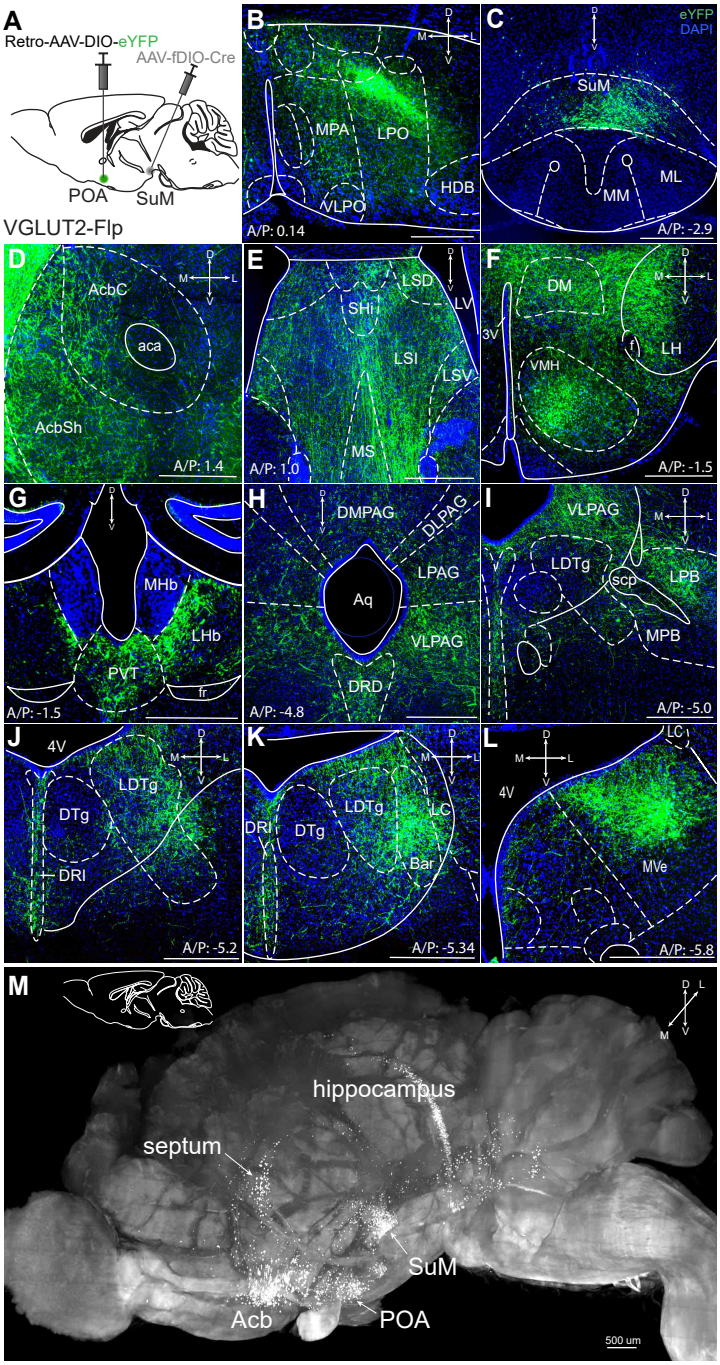

Figure 1. SuM$^{VGLUT2+}$::POA arborize widely in the brain. (A) Schematic of injections of Retro-AAV-DIO-eYFP in to the POA and AAV-fDIO-Cre into the SuM of VGLUT2-Flp mice to label only VGLUT+ SuM neurons that project to the POA. (**B**) Projections of VGLUT2+ SuM neurons labeled with eYFP seen in the POA. (**C**) Cell bodies labeled with eYFP in the SuM. (**D-L**) Arborizing processes from the SuM$^{VGLUT2+}$::POA neurons are seen in multiple brain regions including the (**D**) AcbSh and AcbC; (**E**) lateral septum; (**F**) multiple hypothalamic areas; (**G**) LHb and PVT; (**H**) the PAG and the DRD; (**I**) VLPAG and LPB; (**J**) DRI and LDTg; (**K**) and DRI, and MVePC. (**M**) Light sheet microscopy image of a cleared mouse brain hemisphere, viewed from medial to lateral, showing eYFP labeled neurons in SuM$^{VGLUT2+}$::POA neurons with cell bodies in SuM and processes in areas corresponding to septum, hippocampus, Acb, and POA. (500 µm scale bars)

Abbreviations: *MPA*- medial preotic, *VLPO*- ventral lateral preoptic, *LPO*- lateral preotic, *HDB*- nucleus of the horizontal limb of the diagonal band *AcbSh*- Accumbens shell, *AcbC*- Accumbens core, *Shi*- septohippocampal nucleus, *LSI*- lateral septal nucleus, intermediate part, *LSV*- lateral septal nucleus, ventral part, *LV*- lateral ventricle, *MS*- medial septal nucleus, *LHb*- lateral habenula, *MHb*- medial habenula, *PVT*- paraventricular thalamus, *DM*- dorsomedial hypothalamic nucleus, *LH*- lateral hypothalamic area, *VMH*- ventromedial hypothalamic nucleus, *PAG*- periaqueductal gray, *DMPAG*- dorsomedial periaqueductal gray, *DLPAG*- dorsolateral periaqueductal gray, *LDTg*- laterodorsal tegmental nucleus, *LPAG*- lateral periaqueductal gray, *DRD*- dorsal raphe nucleus, dorsal part, *LPB*- lateral parabrachial nucleus, *MPB*- medial parabrachial, *scp*- superior cerebellar peduncle, *Bar*- Barrington's nucleus, *DTg*- dorsal tegmental nucleus, *DRI*- dorsal raphe, interfascicular part, *LC*- locus coeruleus, MVe- medial vestibular nucleus, *4V*- fourth ventricle

Figure 2

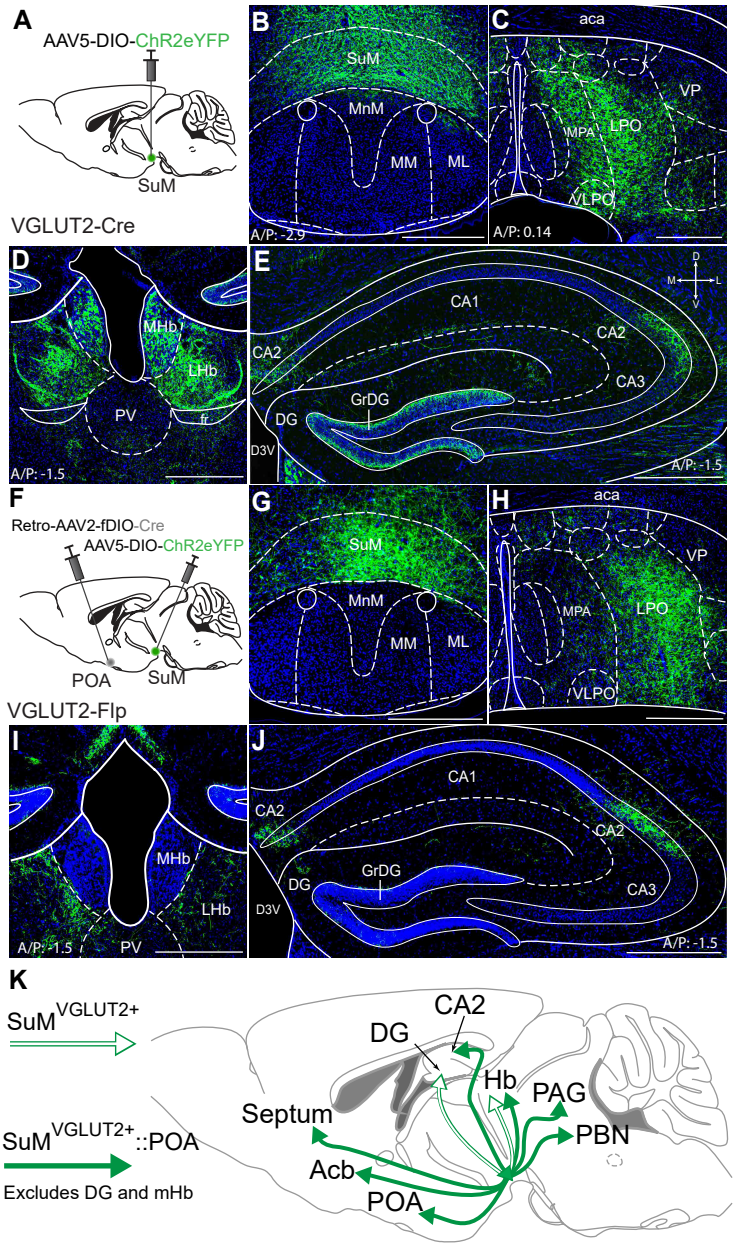

Figure 2. SuM$^{VGLUT2+}$::POA neurons project to a subset of brain regions compared to all SuM$^{VGLUT2+}$ neurons. (**A**) Schematic of injections in VGLUT2-Cre mice of AAV-DIO-ChR2eYFP into SuM. (**B**) eYFP (green) labeled neurons present in SuM and (**C**) processes were observed in the POA. (**D**) Process from SuM VGLUT2+ neurons were also present in MHb, LHb and PVT. (**E**) In hippocampus process were observed in DG and CA2. (**F**) Schematic of injections in VGLUT2-Flp mice of Retro-AAV-fDIO-Cre and AAV-DIO-ChR2eYFP into SuM. (**G-H**) Cells in SuM and process in POA were labeled by ChR2eYFP. (**I**) Labeled processes in LHb were evident but none seen in MHb. (**J**) In hippocampus, labeled processes were present in CA2 but not observed in DG. (500 µm scale bars) (**K**) Schematic summary showing the projection to DG and MHb present in the total SuM VGLUT2+ population (outlined arrows) but absent in the SuM$^{VGLUT2+}$::POA population (filled arrows).

Figure 3

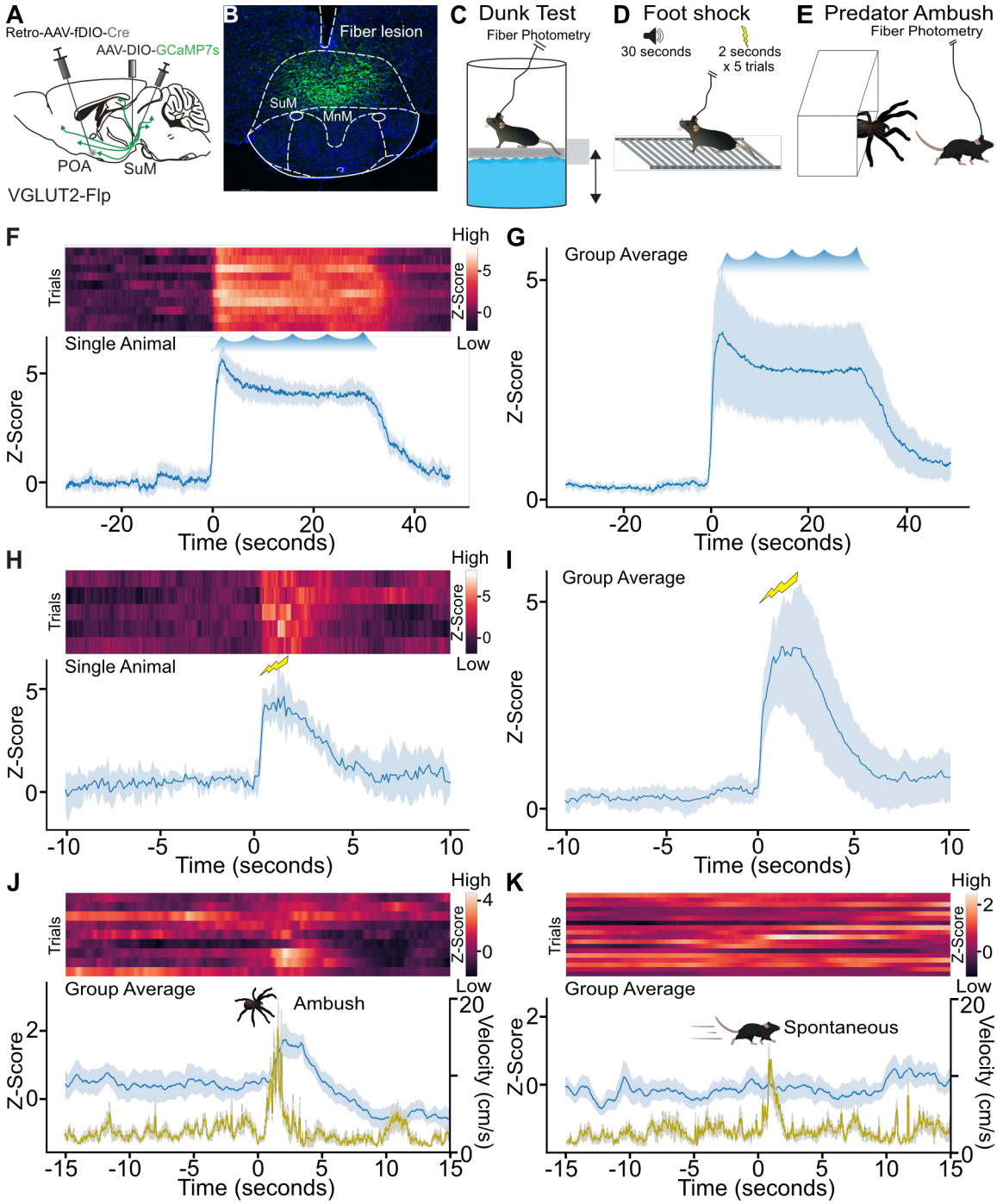

Figure 3. Acute stressors recruit SuM$^{VGLUT2+}$::POA neurons. (**A**) Schematic of VGLUT2-Flp mice injected with AAV-DIO-GCaMP7s in SuM and Retro-AAV-fDIO-Cre in the POA with a (**B**) fiber placed over SuM for fiber photometry recordings from SuM$^{VGLUT2+}$::POA neurons. (**C**) While mice were connected for fiber photometry they were (**C**) subjected to ten 30-second trials of forced swimming, (**D**) to a 2-second foot shock following a 30 second tone for five trials, or (**E**) to mock predator ambushed by a remote-controlled spider. (**F**) Heat map and mean ± 95% CI Z-score for recordings obtained from a single animal during the repeated forced swim showing increase Ca^{2+} signal during the swim session. (**G**) The mean ±95% CI Z-score of 10 trials for all animals (n=8) in the dunk assay. (**H**) Heat map and mean ± 95% CI Z-score for recordings from a single animal during the five shock trials showing increase Ca^{2+} signal. (**I**) Mean ± 95% CI Z-score for recordings of five trials for all animals (n=6) in the foot shock assay. (**J**) Heat map, mean ± 95% CI Z-score (blue), mean ± 95% CI velocity (gold), for recordings obtained from animals (n=9) during the ambush showing an increase in Ca^{2+} signal as the animals flee from the remote-controlled spider with the mean ±95% confidence interval Z- score of 1 trial (ambush) for all 9 animals. (**K**) Heat map, mean (± 95%CI) Z-score (blue), mean (± 95% CI) velocity (gold), for the same mice but ambush in the predator assay. Time frame gated for spontaneous locomotion. Ca^{2+} signal does not increase during spontaneous locomotion. Mean peak velocity was not significantly different.

Figure 4

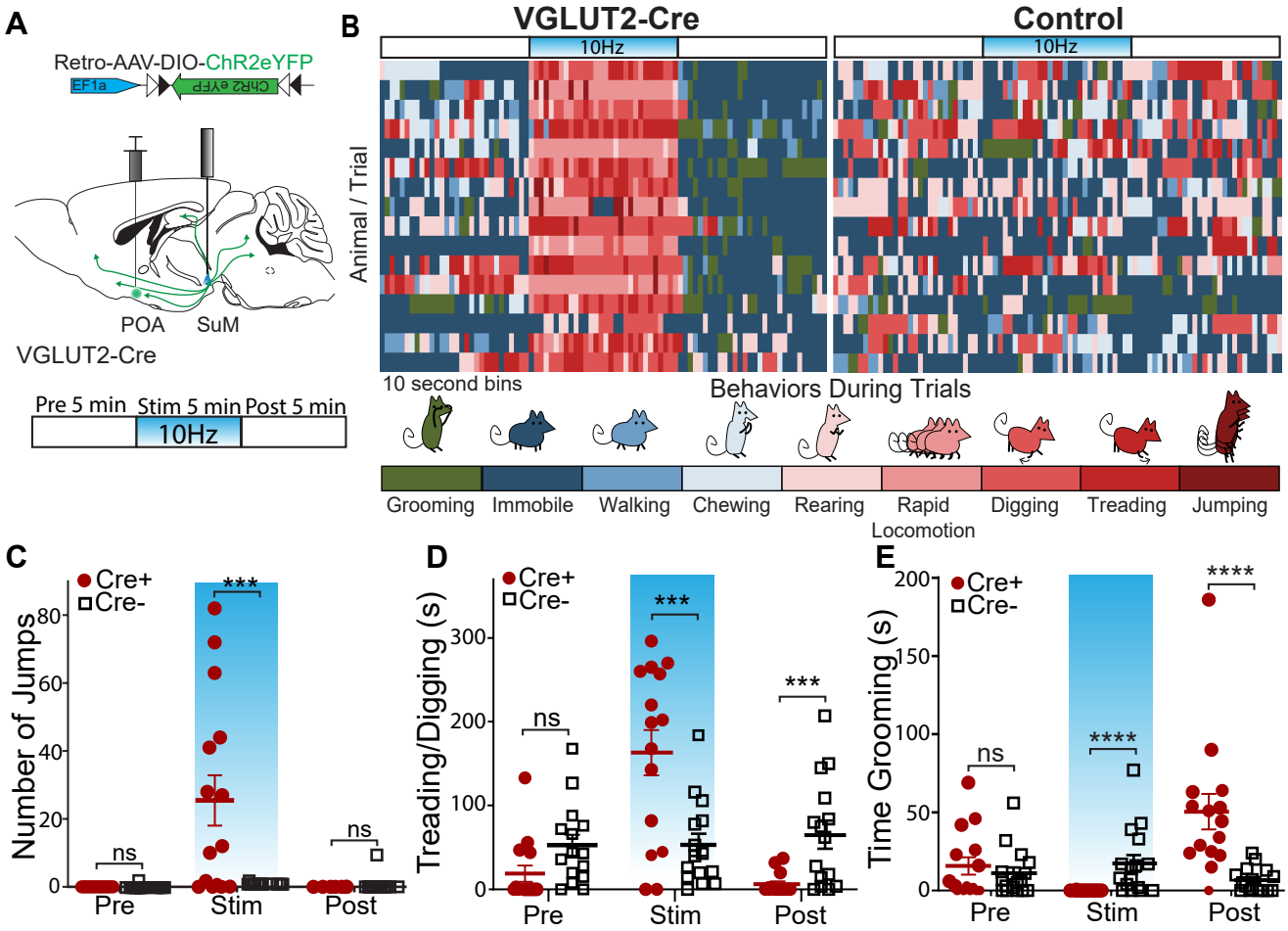

Figure 4. Photostimulation of SuM$^{VGLUT2+}$::POA neurons evokes active coping behaviors. (**A**) Illustration of injections and fiber implant in VGLUT2+ Cre mice and schematic of photostimulation paradigm of 5 min pre, 5 min stimulation, and 5 mins post. Behaviors was evaluated during each epoch. (**B**) For Cre+ (n=16) and Cre- (n=16) mice the behavior in 10 seconds bins was scored based on the predominate behavior displayed during each 10 period for the 15-minute trial into grooming, stationary, walking, chewing, rearing, rapid locomotion, digging (moving bedding towards the tail), treading (move beading forward), and jumping. The graphic show a by animal scoring of the 15-minute trial color coded for each of the behavior categories. (**C**) During the stimulation period Cre+ (n=15) mice show significantly (p=0.0012) greater jumps than Cre- (n=16) mice and jumping behaviors was not significantly different during pre and post stim periods. (**D**) Behavior was also scored for time spent moving beading (digging or treading). Cre+ mice showed significantly (p=0.004) greater time engaging in digging/ treading behaviors during the stimulation period and significantly (p=0.002) less time during the post stimulation period compared to Cre- mice. (**E**) Behavior was also scored for time spent engaging in grooming behaviors and Cre+ mice spent significantly (p<0.001) less time grooming during the stimulation period and significantly (p<0.001) more during the post stimulation period compared to Cre- mice. All data plotted as mean ±SEM

Figure 5

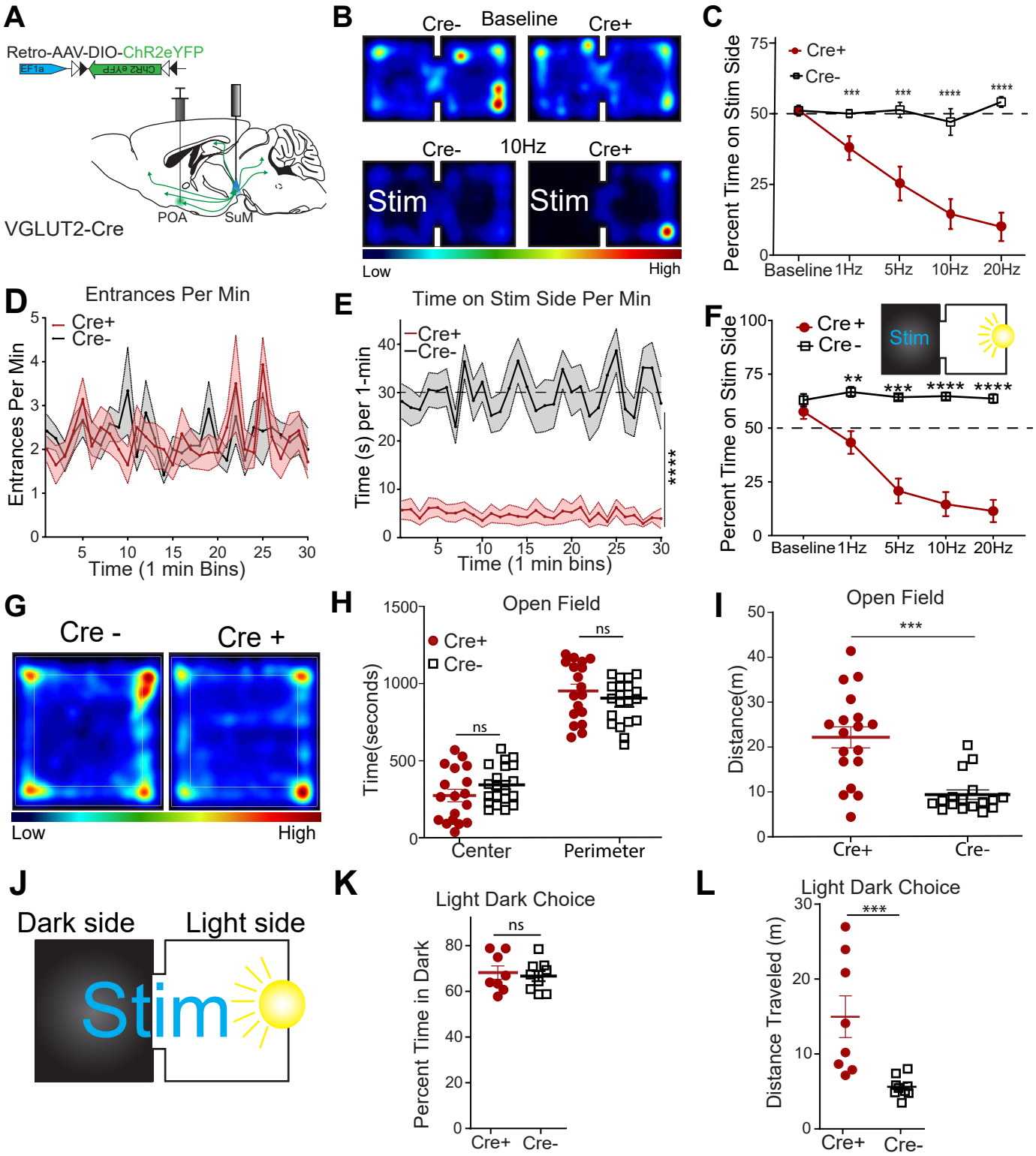
A
Retro-AAV-DIO-ChR2eYFP
EF1a
ChR2 eYFP
POA
SuM
VGLUT2-Cre
B
Cre-
Baseline
Cre+
Cre-
10Hz
Cre+
Stim
Stim
Low
High
C
Percent Time on Stim Side
Cre+
Cre-
Baseline
1Hz
5Hz
10Hz
20Hz
D
Entrances Per Min
Cre+
Cre-
Entrances Per Min
Time (1 min Bins)
E
Time on Stim Side Per Min
Cre+
Cre-
Time (s) per 1-min
Time (1 min bins)
F
Cre+
Cre-
Stim
Percent Time on Stim Side
Baseline
1Hz
5Hz
10Hz
20Hz
G
Cre -
Cre +
Low
High
H
Open Field
Cre+
Cre-
ns
ns
Time(seconds)
Center
Perimeter
I
Open Field
Distance(m)
Cre+
Cre-
J
Dark side
Light side
Stim
K
Light Dark Choice
ns
Percent Time in Dark
Cre+
Cre-
L
Light Dark Choice
Distance Traveled (m)
Cre+
Cre-

Figure 5. Activation of SuM$^{VGLUT2+}$::POA neurons drives aversion but does not promote anxiety-like behavior (**A**) Schematic of injection of Retro-AAV-ChR2eYFP into the POA and placement of a midline optic fiber over SuM. (**B**) Representative heat maps for Cre+ and Cre- mice at baseline (no stim) and 10Hz photostimulation in two-sided arena with photostimulation associated with one side. (**C**) Quantification of time spent of stimulation side for Cre+ (n =19) and control Cre- (n=21) mice showing frequency dependent increase in avoidance of the stimulation side of the area (***p<0.001, ****p<0.0001). (**D**) Mean ±SEM entrances per min (in 1-min bins) to the during 10 Hz stimulation trials were not significantly (p=0.87) different between Cre+ (n=14) and Cre- (n=13) mice. (**E**) Mean time spent on the stimulation side for Cre- and Cre + in 1-minute bins during 10 Hz stimulation trials was significantly (p<0.0001) lower in Cre+ mice. (**F**) (Inset) Diagram of light/dark arena with photo stimulation provided on the dark side of the arena and quantification of time spent on dark (stimulation) side demonstrating that Cre- (n=12) animals show a baseline preference for the dark side of arena that is overcome by photostimulation with Cre+ (n=13) mice spending significantly (**p=0.002, ***p<0.001, ****p<0.0001) less time on the stimulation side. (**G**) Representative heat map of Cre- and Cre+ during 10Hz photostimulation in open field test. (**H**) In open field test time spent in center and perimeter were not significantly different (p=0.19) between Cre+ (n=18) and Cre- (n=17) during 10 Hz photostimulation. (**I**) Distance traveled during open field testing was significantly (p<0.001) increased in Cre+ compared to Cre- mice. (**J**) Schematic of real time light/dark choice testing with stimulation provided at 10Hz throughout the arena. (**K**) Both Cre+ (n=8) and Cre- (n=9) mice showed a preference for the dark portion of the arena but were not significantly (p=0.9) different. (**L**) The total distance traveled by Cre+ mice were significantly (p=0.003) greater than Cre- mice. All data plotted as mean ±SEM.

Figure 6

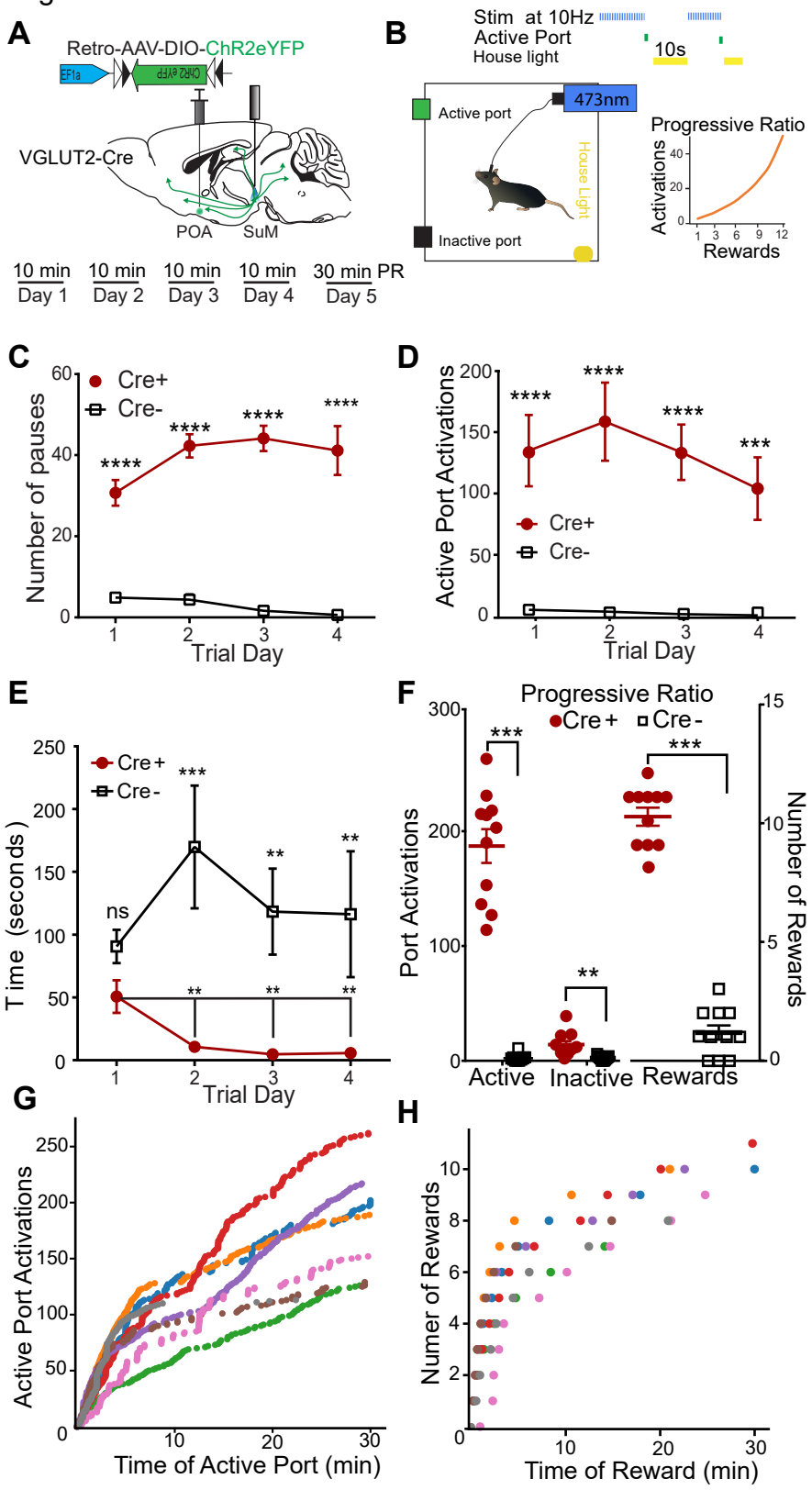

Figure 6. SuM$^{VGLUT2+}$::POA neurons drive can drive instrumental action-outcome operant behavior (**A**) Schematic of injection and implant in VGLUT2+ Cre mice and paradigm of testing in 10-minute trials with 4 days before a progressive ratio (PR) trial on day 5. (**B**) Illustration of the testing paradigm and set up. 10 Hz photostimulation was applied during the trials. Activation of the active port trigger the house light and paused stimulation for 10 seconds. Also shown is the progressive ratio used with number of required port activations per reward on vertical axis and reward number on the horizontal. (**C**) Cre+ mice (n=11) activated the active port triggering significantly (****p<0.0001) more pauses in stimulation than Cre- mice (n=11) mice on all 4 days of testing. (**D**) Cre+ mice activated the port significantly (****p<0.0001, ***p<0.001) than the Cre- mice on all 4 trials. Cre+ activated the active port significantly (p<0.001) on during the fourth trial than the first. (**E**) The time to first activation of the active port was not significantly (p=0.32) different during the first trial but Cre+ mice became significantly (**p<0.01, ***p<0.001) on subsequent trials. (**F**) On the fifth day after four 10-minute trials mice were tested for 30 minutes using a progressive ratio. Cre+ performed significantly (p<0.0001) more active port activations that Cre- mice and activated the inactive port significantly more (p<0.005) times. Cre+ mice also triggered significantly (p<0.001) more pauses in photostimulation that Cre- mice. (**G**) Individual data for a representative cohort of Cre+ mice showing cumulative active port activations by Cre+ mice (n=7) as function of time during the progressive ratio test are shown illustrated on-going engagement of the active port throughout the 30-minute trial. (**H**) The cumulative pauses in photostimulation (rewards) earned as a function of time during the progressive ratio trial are show for individual Cre+ mice. Mice earned between 7 and 11 pause reward during the trial. All data plotted as means ±SEM.

Figure 7

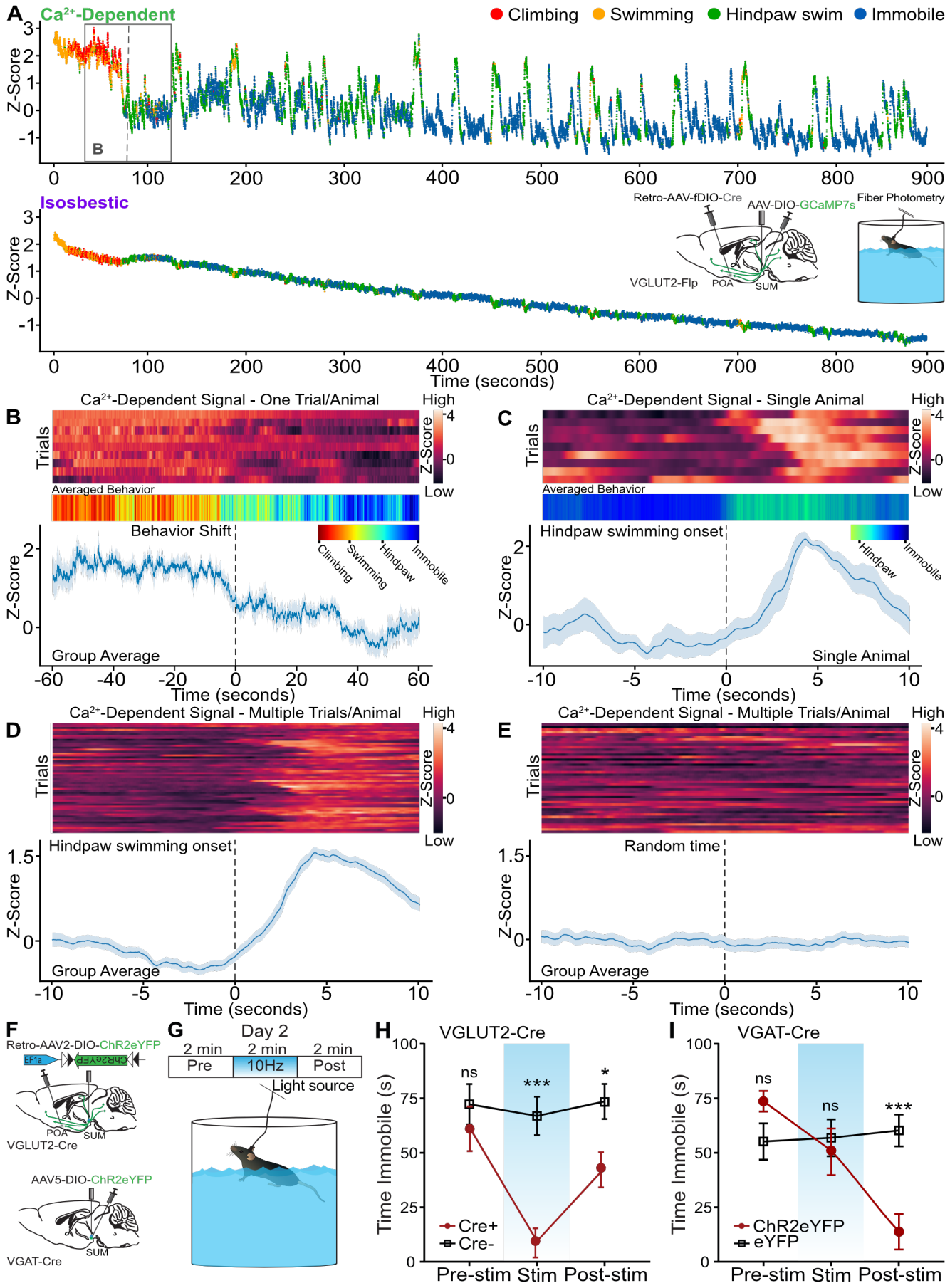
A
Ca2+-Dependent
Climbing
Swimming
Hindpaw swim
Immobile
Z-Score
B
Isosbestic
Retro-AAV-fDIO-Cre
AAV-DIO-GCaMP7s
Fiber Photometry
VGLUT2-Flp
POA
SUM
Time (seconds)
B
Ca2+-Dependent Signal - One Trial/Animal
Trials
Z-Score
High
Low
Averaged Behavior
Behavior Shift
Climbing
Swimming
Hindpaw
Immobile
Group Average
Time (seconds)
C
Ca2+-Dependent Signal - Single Animal
Hindpaw swimming onset
Single Animal
D
Ca2+-Dependent Signal - Multiple Trials/Animal
Hindpaw swimming onset
Group Average
E
Ca2+-Dependent Signal - Multiple Trials/Animal
Random time
Group Average
F
Retro-AAV2-DIO-ChR2eYFP
EF1a
ChR2eYFP
POA
SUM
VGLUT2-Cre
AAV5-DIO-ChR2eYFP
SUM
VGAT-Cre
G
Day 2
2 min
2 min
2 min
Pre
10Hz
Post
Light source
H
VGLUT2-Cre
Time Immobile (s)
ns
***
*
Cre+
Cre-
Pre-stim
Stim
Post-stim
I
VGAT-Cre
Time Immobile (s)
ns
ns
***
ChR2eYFP
eYFP
Pre-stim
Stim
Post-stim

Figure 7. SuM$^{VGLUT2+}$::POA neurons are recruited during active coping and activation is sufficient drive a switch to active coping. (**A**) Color coded per video frame (dot color) behavior combined with normalized Ca^{2+} dependent and isosbestic fiber photometry signals. Scoring and analysis of climbing, swimming, hindpaw swimming, and immobility was completed using deep learning based classification and quantification (LabGym) of recorded behavior. Inset shows injection and implants and behavioral assay. Box highlights the time frame shown in B. (**B**) Heat maps for recordings obtained mice (n=9) during forced swim, averaged color-coded behaviors, and mean ±SEM Z-score of Ca^{2+} dependent signal for 2-min period around behavioral shift from climbing and swimming to hindpaw swimming and immobility. (**C**) Representative heat map, averaged behavior, and mean ±SEM Z-score of Ca^{2+} dependent signal for 20-second window around onset of hindpaw swim from a representative animal. (**D**) Representative heat map and mean ±SEM Z-score of Ca^{2+} dependent signal for 20-second window around onset of hindpaw swim from for events from nine mice. Engaging in hindpaw swim correlates with brief increase in Ca^{2+} signal. (**E**) Representative heat map and mean ±SEM Z-score of Ca^{2+} dependent signal for 20-second window around random time points. (**F**) Schematic of injection and implant in VGLUT2-Cre or VGAT-Cre mice. (**G**) Illustration of testing paradigm on second of forced swim test following 15-minute swim on first day. (**H**) The average time spent immobile during the pre-stimulation period was not significantly (p=0.48) different. During 10 Hz photostimulation VGLUT2-Cre+ mice engaged in vigorous swimming and the time spent immobile was significantly (***=p<0.001) less than Cre- mice. In the post-stimulation period, the time spent immobile remained significantly (*=0.016) lower in Cre+ mice compared to Cre-. (**I**) In VGAT-Cre+ mice expressing ChR2 (n=10), the average time spent immobile during the pre-stimulation period was not significantly (p=0.08) different compered to eYFP controls. Photostimulation did not significantly increase time immobile (p=0.64). However, there was a significant (*** p=0.0004) decrease in the time spent immobile compared in the post-stimulation period.

Figure 8

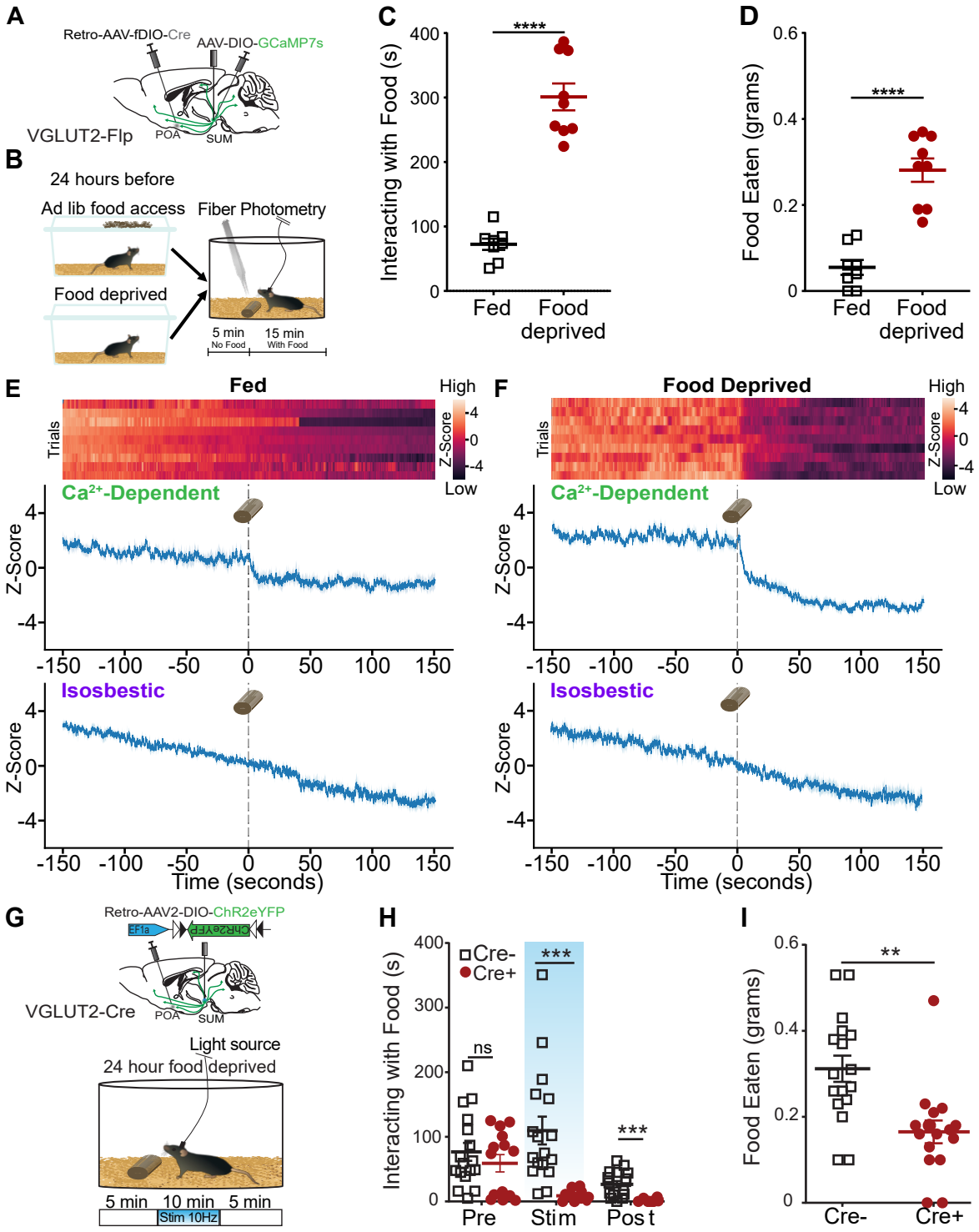
A
Retro-AAV-fDIO-Cre
AAV-DIO-GCaMP7s
VGLUT2-Flp
POA
SUM
B
24 hours before
Ad lib food access
Fiber Photometry
Food deprived
5 min
No Food
15 min
With Food
C
Interacting with Food (s)
****
Fed
Food deprived
D
Food Eaten (grams)
****
Fed
Food deprived
E
Fed
Trials
High
Z-Score
Low
Ca2+-Dependent
Isosbestic
Z-Score
Time (seconds)
F
Food Deprived
Trials
High
Z-Score
Low
Ca2+-Dependent
Isosbestic
Z-Score
Time (seconds)
G
Retro-AAV2-DIO-ChR2eYFP
EF1a
ChR2eYFP
VGLUT2-Cre
POA
SUM
Light source
24 hour food deprived
5 min
10 min
5 min
Stim 10Hz
H
Interacting with Food (s)
Cre-
Cre+
ns
***
***
Pre
Stim
Post
I
Food Eaten (grams)
**
Cre-
Cre+

Figure 8. Consummatory behavior suppresses SuM$^{VGLUT2+}$::POA neuron activity and SuM$^{VGLUT2+}$::POA neuron blocks food consumption. (**A**) Schematic of injections in VGLUT2-Flp mice with AAV-DIO-GCaMP7s in SuM and Retro-AAV-fDIO-Cre in the POA and a fiber placed over SuM. (**B**) Mice were given ad lib food access or food deprived for 24 hours prior to testing. After being placed in arena and allowed to habituate mice were given a 20-minute trial divided into 5 mins baseline and 15 mins after a chow pellet was added to the arena. (**C**) Food deprived mice (n=9) spent significantly ($p< 0.001$) more time interacting with the food pellet and (**D**) ate significantly ($p<0.001$) more than in the fed state. (**E**) Heat map and mean ±SEM z-scores for Ca^{2+} dependent and isosbestic signals for recordings obtained from 9 animals show a small drop in (**E**) fed mice state compered to a sharp decrease in Ca^{2+} activity after the introduction of the food pellet following addition in (**F**) food deprivation. (**G**) Mice were fasted for 24 hours prior to testing and the schematize 20 min paradigm was used. Following food deprivation animals were given access a chow pellet. The trial was divided in to a 5-minute pre- and post-stimulation periods with 10-minute period of stimulation. (**H**) The time spent interacting with the food was quantified for each period. Cre+ (n=16) and Cre- (n=17) mice both rapidly engaged with the food pellet and the average time spent interacting was not significantly ($p=0.37$) different. During the stimulation period and the post stimulation period the average time interacting with the food was significantly ($p=0.0002$, $p=0.0001$) lower in Cre+ mice compared to Cre- mice. (**I**) The food eaten during the total trial was calculated based on pellet weights and on average Cre+ mice ate significantly ($p=0.001$) less food during the trial than Cre- mice. (**$p=0.001$, ***$p<0.001$, ****$p<0.0001$)

Supplemental Figure 1

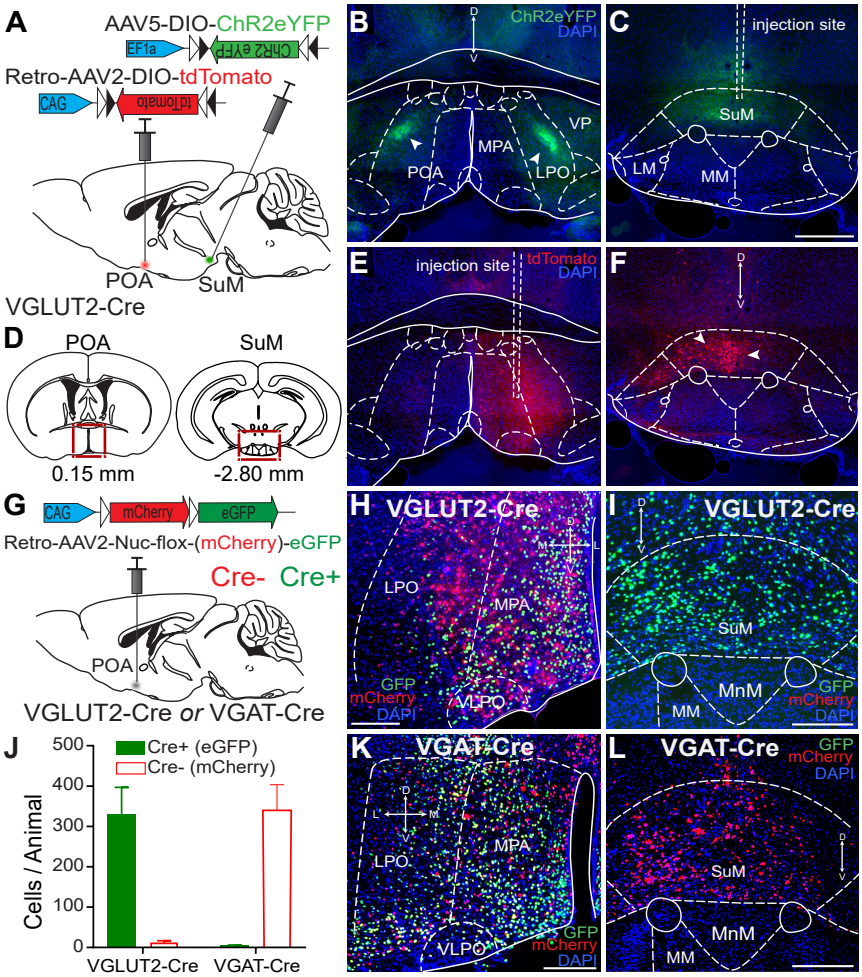

Supplemental Figure 1. SuM$^{VGLUT2+}$ neurons project to the preoptic area of the hypothalamus and are not VGAT+. (**A**) Schematic of injections into VGLUT2-Cre mice of Retro-AAV-DIO-tdTomato into the POA and AAV-DIO-ChR2eYFP into the SuM. (**B and C**) Projections of VGLUT2+ SuM neurons and evident in the POA with dense labeling in LPO and the site of viral injection in SuM (500um scale bar). (**D**) The brain regions, POA and SuM, shown in (B,C, E and F). (**E and F**) Cell bodies of VGLUT2+ SuM neurons are evident in Sum with injection of Retro-AAVs in POA. (**G**) Schematic of injection in POA of fluorophore switching construct in Retro-AAAV in VGLUT2-Cre or VGAT-Cre mice. (**H and I**) Labeling of Cre- (red) and Cre+ neurons in POA but only Cre+ seen in SuM of VLGUT2-Cre mice showing all SuM::POA neurons are VGLUT2+. (**J**) Quantification of labeling of Cre+ and Cre- cells in SuM following injections in POA in VGLUT2-Cre and VGAT-Cre mice. (**K and L**) Labeling of Cre- (red) and Cre+ neurons in POA but only Cre- seen in SuM of VGAT-Cre mice. (100um scale bar)

Supplemental Figure 2

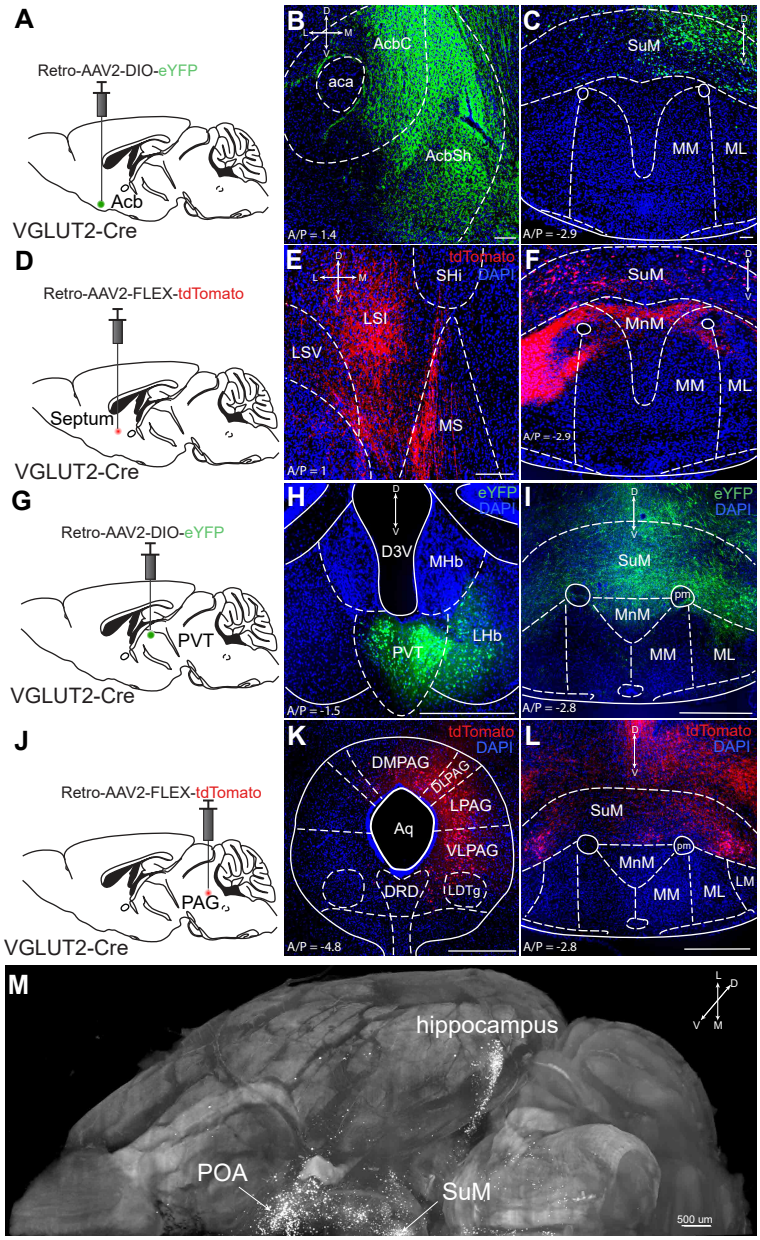

Supplemental Figure 2. Retrograde verification of projection targets of SuM$^{VGLUT2+}$::POA. (**A, D, G, and J**) Schematic showing the injection sites of Retro-AAV's in VGLUT2-Cre mice. (**B-C**) In VGLUT2-Cre mice injection of Retro-AAV-DIO-eYFP unilaterally in the (**B**) accumbens nucleus resulted in labeling of cell bodies in (**C**) SuM. (E-F) Similarly, injection of Retro-AVV-DIO-tdTomato into (**E**) septum resulted in labeling of cell bodies in (**F**) SuM. (**H-I**) injection of Retro-AAV-DIO-eYFP targeting the (**H**) PV and LHb resulted in cell bodies in (**I**) SuM being labeled with eYFP. (**K-L**) Retro-AVV-DIO-tdTomato injected into (**K**) PAG labeled cells in (**L**) SuM. (**M**) The cleared brain hemisphere from a VGLUT2-Flp mouse injected in the POA with injected Retro-AAV-DIO-eYFP show in Figure 2M displayed from a perspective of ventral to dorsal showing cells labeled in SuM and processes extending widely including in the hippocampus and POA. (100 and 500 µm scale bars)

Supplemental Figure 3

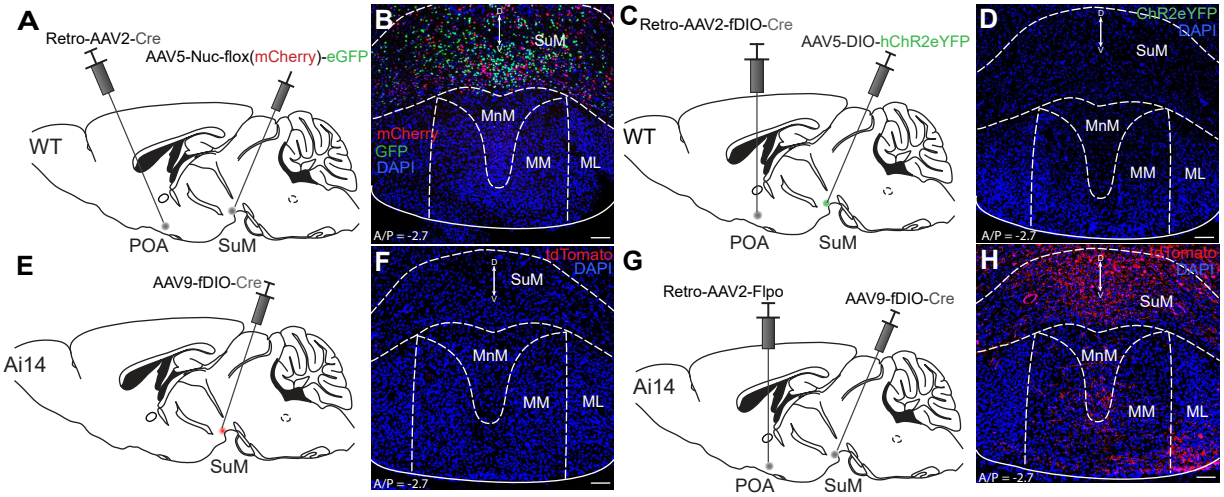

Supplemental Figure 3. Combinatorial viral and genetic approach is effective with minimal background. (**A**) Schematic of injection of Retro-AAV-Cre into the POA and AAV-Nuc-flox(mCherry)-eGFP into the SuM of WT mice. (**B**) In SuM eGFP (green) Cre positive and mCherry (red) Cre negative labeled neurons are seen based on expression of Cre mediated by POA injected retrograde AAV constructs showing SuM::POA neurons are a subset of all cells in SuM. (**C and D**) In wildtype mice injected in POA with Retro-AAV-fDIO-Cre and in SuM with AAV-DIO-ChR2eYFP expression of ChR2eYFP (green) is not seen. (**E-H**) In Ai14 reporter mice injected with AAV-fDIO-Cre into SuM tdTomato expression is not observed unless Retro-AAV2-Flp is injected. (100 µm scale bars)

Supplemental Figure 4

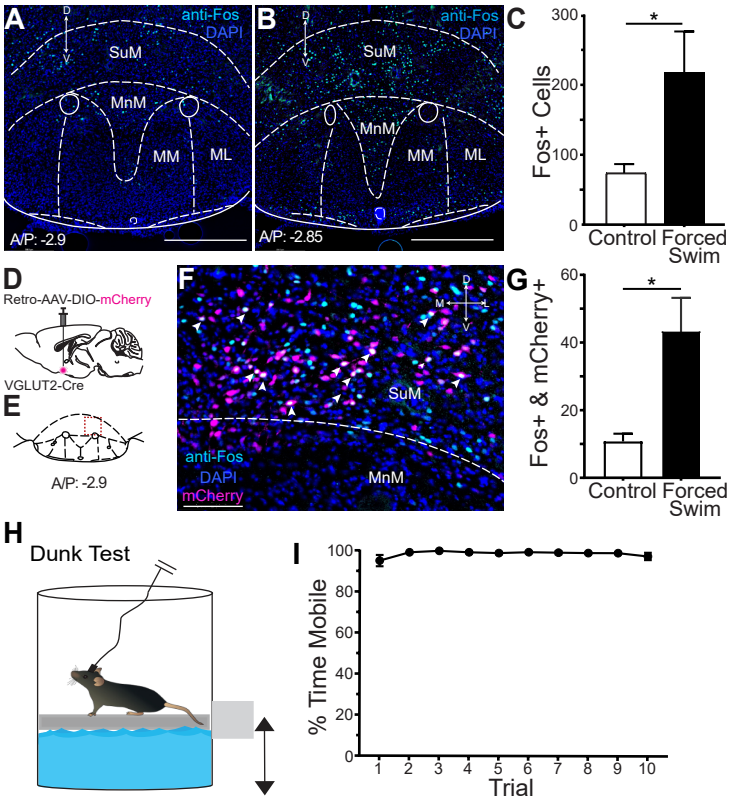

Supplemental Figure 4. SuM$^{VGLUT2+}$::POA neurons show Fos induction after FST and dunk test evokes active coping. Sections of brains from mice (**A**) left in the home cage or (**B**) subjected to 15 minutes of forced swimming 90 min prior to sacrifice were probed with anti-Fos antibodies (cyan) showed (scale bars 500µm) (**C**) a significant (p= 0.029) increase in them mean ±SEM number of anti-Fos labeled neurons in brains from mice subjected to force swim (n=5) compared to control mice (n=4). (**D**) In VLGUT2-Cre mice Retro-AAV-DIO-mCherry was injected in the POA of mice (n=5) subjected to 15 minutes forced swim. (**E**) Region of SuM shown with higher magnification in (**F**) where SuM$^{VGLUT2+}$::POA neurons labeled by mCherry show overlap with cells (arrows) labeled by anti-Fos. (Scale bar 100µm) (**G**) A significant increase (p= 0.016) in the number of VGLUT2+ cells labeled with mCherry and anti-Fos in mice subjected to forced swim. (**H**) Mice subjected to 10 30-second trials of “dunk” forced swimming. (**I**) Quantitation of average time mobile for every 30-second trial during “dunk” forced swim.

Supplemental Figure 5

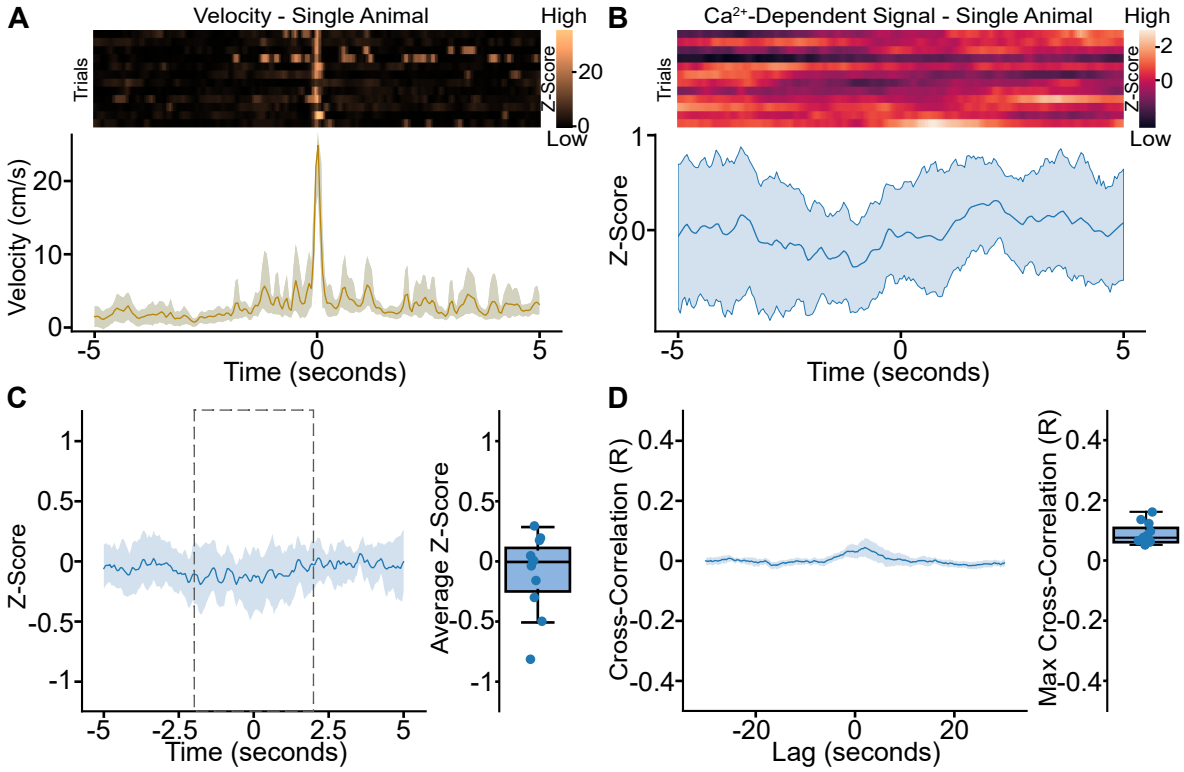

Supplemental Figure 5. SuM$^{VGLUT2+}$::POA neurons are not recruited during increased locomotor activity in the absence of acute stressor. (**A**) Heat maps showing velocity for 12 episodes of rapid locomotion from a representative animal during free movement in open field with mean ±95% CI for the trials. (**B**) For that same animal heat map of Ca^{2+} dependent signal was analyzed during average peak velocity showing no change in activity during peak velocity. Representative heat map for a single animal with the mean ±95% confidence interval of the 12 trials for same animal. (**C**) Mean ±95% confidence interval for Z-score of 12 trials for all 13 animals and Boxplot for average Z-score. (**D**) Cross-correlation analysis shows no correlation between Ca^{2+} signal from SuM$^{VGLUT2+}$::POA neurons spontaneous velocity increases.

Supplemental Figure 6

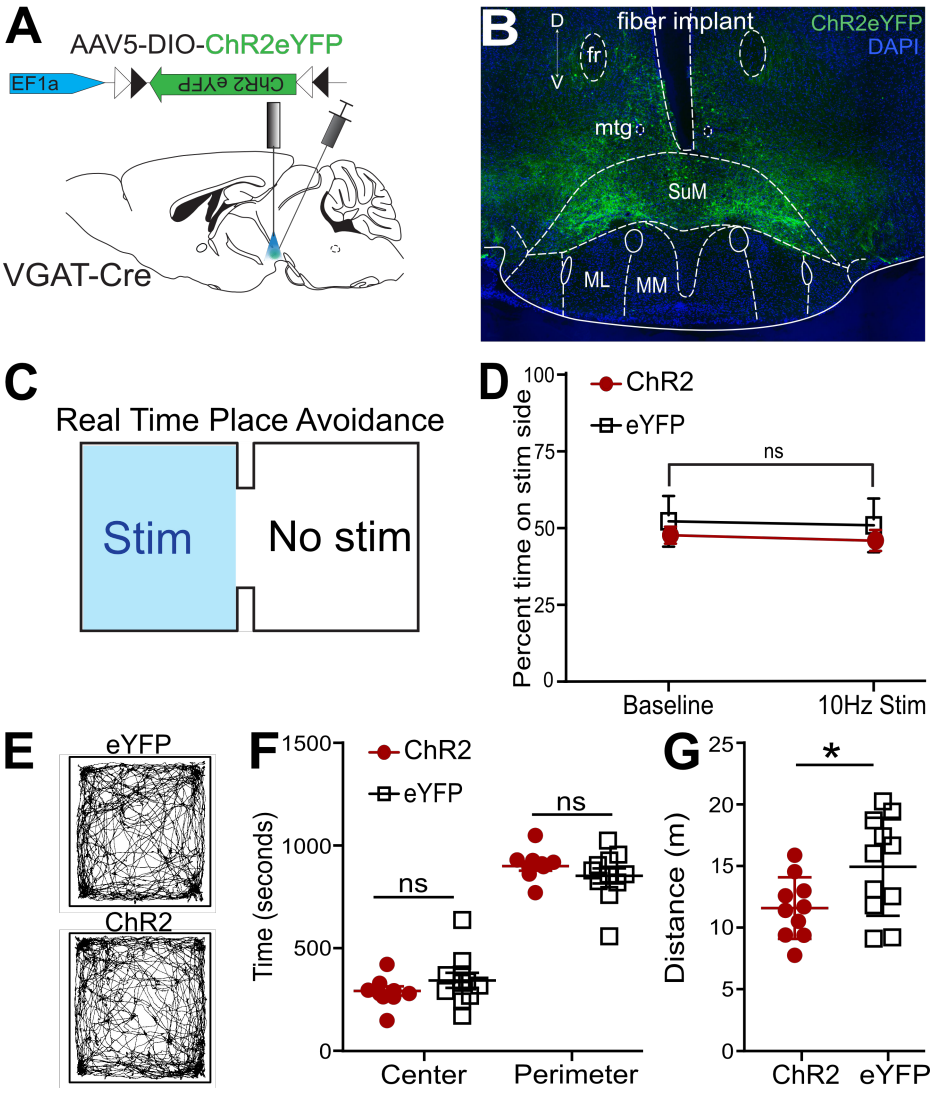

Supplemental Figure 6. GABAergic neurons in SuM do not drive place preference. (**A**) Schematic of viral injection into VGAT-Cre mice in SuM. (**B**) VGAT+ neurons labeled and outline of implanted fiber. (**C**) Real-time arena showing the pair of photostimulation on one side of the arena. (**D**) Photostimulation at 10Hz did not drive a significant place preference. (eYFP (control) n=26 and ChR2=26). All data plotted as mean ±SEM. (**E**) Representative path traces of VGAT-Cre mice with ChR2 or eYFP (control) in open field testing. (**F**) No significant differences in center or perimeter time when comparing the ChR2eYFP expressing to controls VGAT-Cre mice. (**G**) Chr2eYFP expressing mice traveled slightly but significantly (p=0.034) less distance compered to control.